Molecular Cell

Pseudouridine synthases modify human pre-mRNA co-transcriptionally and affect pre-mRNA processing

Graphical abstract

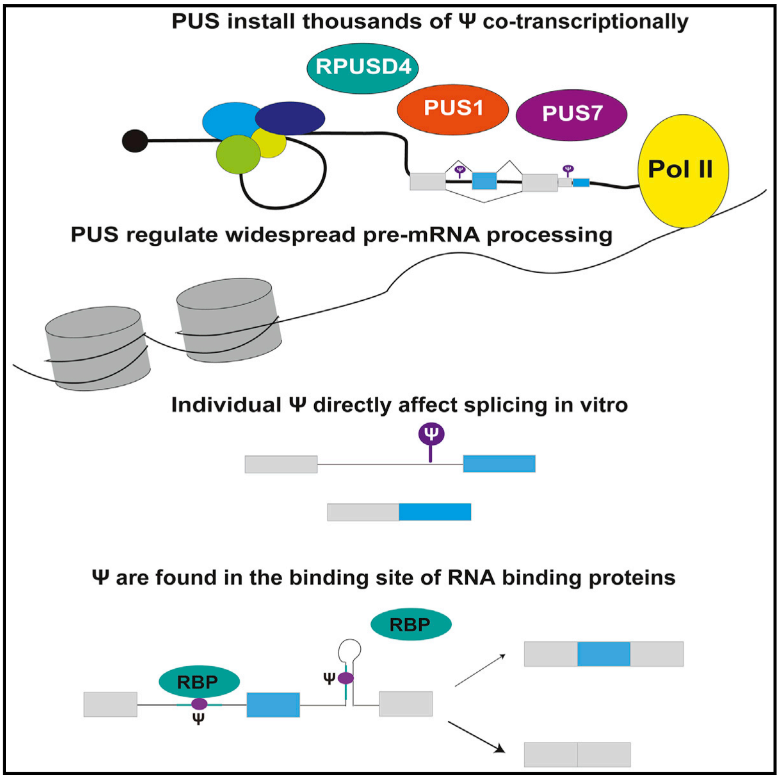
PUS install thousands of Ψ co-transcriptionally
RPUSD4
PUS1
PUS7
Pol II
Ψ
PUS regulate widespread pre-mRNA processing
Individual Ψ directly affect splicing in vitro
Ψ
Ψ are found in the binding site of RNA binding proteins
RBP
RBP
Ψ
Ψ

Highlights

- Pseudouridine RNA modifications are installed cotranscriptionally
- Pre-mRNA pseudouridines are enriched in alternatively spliced regions
- A single pseudouridine is sufficient to affect splicing efficiency *in vitro*
- Three human pseudouridine synthases mediate widespread alternative pre-mRNA processing

Authors

Nicole M. Martinez, Amanda Su, Margaret C. Burns, ..., Shashank Sathe, Gene W. Yeo, Wendy V. Gilbert

Correspondence

geneyeo@ucsd.edu (G.W.Y.),
wendy.gilbert@yale.edu (W.V.G.)

In brief

By profiling pseudouridines in chromatin-associated RNA, Martinez et al. demonstrate that pseudouridylation takes place cotranscriptionally in pre-mRNA. Multiple pseudouridine synthases directly modify pre-mRNA sequences in high-throughput biochemical assays. The depletion of pre-mRNA-modifying PUS, in turn, reveals a role for PUS in widespread pre-mRNA processing, including alternative splicing and 3′ end processing.

Martinez et al., 2022, Molecular Cell *82*, 1–15
February 3, 2022 © 2021 Elsevier Inc.
https://doi.org/10.1016/j.molcel.2021.12.023

CellPress

Please cite this article in press as: Martinez et al., Pseudouridine synthases modify human pre-mRNA co-transcriptionally and affect pre-mRNA processing, Molecular Cell (2021), https://doi.org/10.1016/j.molcel.2021.12.023

Molecular Cell

CellPress

Article

Pseudouridine synthases modify human pre-mRNA co-transcriptionally and affect pre-mRNA processing

Nicole M. Martinez,[1] Amanda Su,[1] Margaret C. Burns,[2,3,4] Julia K. Nussbacher,[2,3,4] Cassandra Schaening,[5] Shashank Sathe,[2,3,4] Gene W. Yeo,[2,3,4,*] and Wendy V. Gilbert[1,6,*]

[1]Yale School of Medicine, Department of Molecular Biophysics & Biochemistry, New Haven, CT 06520, USA
[2]Department of Cellular and Molecular Medicine, University of California, San Diego, La Jolla, CA 92037, USA
[3]Stem Cell Program, University of California, San Diego, La Jolla, CA 92037, USA
[4]Institute for Genomic Medicine, University of California, San Diego, La Jolla, CA 92037, USA
[5]Department of Biology, Massachusetts Institute of Technology, Cambridge, MA 02142, USA
[6]Lead contact
*Correspondence: geneyeo@ucsd.edu (G.W.Y.), wendy.gilbert@yale.edu (W.V.G.)
https://doi.org/10.1016/j.molcel.2021.12.023

SUMMARY

Pseudouridine is a modified nucleotide that is prevalent in human mRNAs and is dynamically regulated. Here, we investigate when in their life cycle mRNAs become pseudouridylated to illuminate the potential regulatory functions of endogenous mRNA pseudouridylation. Using single-nucleotide resolution pseudouridine profiling on chromatin-associated RNA from human cells, we identified pseudouridines in nascent pre-mRNA at locations associated with alternatively spliced regions, enriched near splice sites, and overlapping hundreds of binding sites for RNA-binding proteins. *In vitro* splicing assays establish a direct effect of individual endogenous pre-mRNA pseudouridines on splicing efficiency. We validate hundreds of pre-mRNA sites as direct targets of distinct pseudouridine synthases and show that PUS1, PUS7, and RPUSD4—three pre-mRNA-modifying pseudouridine synthases with tissue-specific expression—control widespread changes in alternative pre-mRNA splicing and 3′ end processing. Our results establish a vast potential for co-transcriptional pre-mRNA pseudouridylation to regulate human gene expression via alternative pre-mRNA processing.

INTRODUCTION

Pseudouridine is the most abundant modified nucleotide in RNA, and the pseudouridylation of the noncoding RNAs of the translation and splicing machineries is important for their functions. Recent transcriptome-wide methods for the detection of pseudouridine (Ψ) revealed that mRNAs in yeast and human cells contain pseudouridines that are dynamically regulated in response to cellular stress (Carlile et al., 2014; Lovejoy et al., 2014; Schwartz et al., 2014; Li et al., 2015). However, although the roles of other mRNA modifications have been uncovered, such as that of N6-methyladenosine (m6A) in regulating splicing, export, translation, and decay, the endogenous functions of pseudouridine in mRNA are largely unknown (Gilbert et al., 2016; Roundtree et al., 2017; Martinez and Gilbert, 2018).

The potential functions of RNA modifications are constrained when the modification is installed during RNA biogenesis. Because previous studies profiled pseudouridines in mature poly(A)+ mRNAs (Carlile et al., 2014; Lovejoy et al., 2014; Schwartz et al., 2014; Li et al., 2015), it was unknown when mRNA becomes pseudouridylated and which steps of the mRNA life cycle are affected by pseudouridines. In yeast, most mRNA pseudouridines have been genetically assigned to two conserved pseudouridine synthases (PUSs), Pus1 and Pus7 (Carlile et al., 2014; Schwartz et al., 2014), which are nuclear-localized during normal growth (Huh et al., 2003). Human PUS enzymes that have been reported to pseudouridylate mRNA targets (Li et al., 2015; Safra et al., 2017; Carlile et al., 2019) also localize to the nucleus or have nuclear isoforms (Fernandez-Vizarra et al., 2007; Ji et al., 2015; Safra et al., 2017). Furthermore, PUS7 has been shown to be chromatin-associated and copurifies with active Pol II promoters and enhancers (Ji et al., 2015). Pseudouridines are present in nuclear-resident ncRNAs (Carlile et al., 2014; Schwartz et al., 2014). Thus, human PUS enzymes are present and active in the nucleus where they could target pre-mRNA. Because artificial RNA pseudouridylation has been shown to affect RNA-RNA (Newby and Greenbaum, 2001; Hudson et al., 2013; Kierzek et al., 2014) and RNA-protein interactions (Chen et al., 2010; Delorimier et al., 2017; Vaidyanathan et al., 2017) that are known or likely to be relevant to splicing, we hypothesized that human PUS enzymes pseudouridylate nascent pre-mRNA in which they could function in nuclear pre-mRNA processing.

Here, we used single-nucleotide resolution pseudouridine profiling, Pseudo-seq (Carlile et al., 2014, 2015), on chromatin-associated nascent RNA to discover thousands of candidate pseudouridines in the pre-mRNA from the human hepatocellular carcinoma cell line HepG2. These pseudouridines are significantly enriched in the introns flanking sites of alternative splicing, suggesting regulatory potential. Consistently, we identified widespread differences in alternative splicing in response to the genetic manipulation of pre-mRNA pseudouridylating enzymes PUS1, PUS7, and RPUSD4. Furthermore, we showed that site-specific installation of a single endogenous pseudouridine is sufficient to directly influence splicing *in vitro*. We also observed significant cotranscriptional deposition of pseudouridines in 3′ UTRs of pre-mRNAs and demonstrated prevalent PUS-dependent alternative cleavage and polyadenylation. Finally, pseudouridines overlap the experimentally validated binding sites of dozens of RNA-binding proteins (RBPs) interrogated by eCLIP (enhanced UV crosslinking followed by immunoprecipitation), providing a mechanistic link to altered pre-mRNA processing.

RESULTS

Pre-mRNA is pseudouridylated cotranscriptionally in human cells

To determine if pseudouridine is added to pre-mRNA cotranscriptionally, we isolated chromatin-associated RNA from the hepatocellular carcinoma cell line HepG2 by a biochemical cellular fractionation that enriches for intron-containing unspliced pre-mRNA (Figure 1A) (Khodor et al., 2011; Bhatt et al., 2012). The majority (74%) of pre-mRNA sequencing reads mapped to introns, and the read coverage of introns and exons was relatively uniform, demonstrating an efficient capture of intronic reads from unspliced pre-mRNA (Figure 1A). This result contrasts with the primarily exonic reads observed in poly(A)+ mRNA (Figure 1A). We then performed Pseudo-seq (Carlile et al., 2014) to identify the locations of pseudouridine in chromatin-associated RNA. In Pseudo-seq, pseudouridines are selectively modified with the chemical *N*-cyclohexyl-N′-(2-morpholinoethyl)carbodiimide metho-p-toluenesulfonate (CMC). The bulky covalent CMC-pseudouridine adduct blocks reverse transcriptase and allows for the sequencing-based detection of pseudouridines from truncated cDNAs (Figure 1B). By design, Pseudo-seq detects only modification sites where a substantial fraction of the RNA is modified. Because pseudouridine-containing RNAs are not pre-enriched during the Pseudo-seq protocol, high stoichiometry pseudouridylation is required to generate a block to reverse transcription that is sufficiently penetrant to produce detectable peaks of Pseudo-seq signal (Carlile et al., 2015), which is the difference between the normalized reads from the CMC condition and that from the mock-treated control (Figure 1C). Using this approach, the Pseudo-seq signal identified known pseudouridine sites in ribosomal RNA (rRNA) with high sensitivity, specificity, and reproducibility from the chromatin-associated RNA samples (Figures 1D and S1A; Table S1A). We generated data on 11 biological replicates of chromatin-associated RNA to add a stringent reproducibility filter to our site calling and identify high-confidence sites of pre-mRNA modification (Figure 1C).

We identified expected sites in nascent rRNA corresponding to known positions in the mature rRNA sequences with an observed false-positive rate of 0.01 and false discovery rate (FDR) of 0.152 (Figure S1A; Table S1A). These results are consistent with the prevailing hypothesis that rRNA pseudouridines are added cotranscriptionally, as has been shown for 2′-O-methylation in yeast (Koš and Tollervey, 2010; Birkedal et al., 2015). Intriguingly, pseudouridine profiling of chromatin-associated RNA allowed us to detect the precursor regions in pre-rRNA and identify putative sites of pseudouridylation in these regions (Table S1A). These sites have complementarity to human snoRNAs that are predicted by snoGPS (Schattner et al., 2005) to direct their modification (Table S1A). Hundreds more novel pseudouridines were found in nuclear-resident noncoding RNAs that interact with chromatin, including the small nucleolar RNAs (snoRNAs), small cajal body-specific RNAs (scaRNAs), and long noncoding RNAs lncRNAs (Figure 1F; Table S1B). These previously unknown sites were called based on the observation of the highly reproducible enrichment of CMC-dependent read 3′ ends (STAR Methods) using criteria that have previously generated site lists with high confirmation rates (>61%) in independent studies (Carlile et al., 2014, 2019; Khoddami et al., 2019), including using completely orthologous chemistry for pseudouridine detection (Khoddami and Cairns, 2013; Khoddami et al., 2019) (Figures S1C–S1F; Table S1D). Cell-type-specific pseudouridylation and distinct capture biases from technical approaches (e.g., Figure S1D) influence which sites can be detected.

Based on these criteria, the analysis of the Pseudo-seq signal in pre-mRNA conservatively identified thousands of candidate pseudouridines, with the majority of pseudouridines being found in introns (Figures 1B, 1C, and 1F; Table S1C). This number likely represents a small fraction of the total pseudouridines in pre-mRNA since only ~1% of uridines in the nascent transcriptome had sufficient sequencing depth to meet our pseudouridine calling criteria (STAR Methods). The distribution of pre-mRNA pseudouridines among gene features including introns, exons, 5′-UTRs, and 3′-UTRs was similar to the distribution of uridines passing the minimum read cutoff for pseudouridine detection (Figure 1F). This apparently widespread modification of pre-mRNA introns with pseudouridine contrasts with the observed distribution of m6A, another abundant mRNA modification added to pre-mRNA, which is found primarily in exons (90% of m6As), despite a similar distribution of intronic to exonic reads as observed in our study (Ke et al., 2017). These results reveal that pseudouridylation is a cotranscriptional process that results in the prevalent installation of pseudouridines in pre-mRNA, endowing this modification with the potential to affect nuclear pre-mRNA processing steps such as splicing and 3′ end processing.

Comparing the pseudouridine sites in nascent pre-mRNA from HepG2 cells with the sites previously identified in poly(A)+ mRNA from HeLa revealed both similarities and differences. Of the 18 HeLa mRNA sites that were expressed at sufficient levels to assess pseudouridylation in HepG2 pre-mRNA, 5 were called in chromatin-associated RNA, suggesting that they are added early and conserved across cell types (Figure 1E). Other sites that were expressed at levels with sufficient coverage in both cell lines were present exclusively in either HeLa or HepG2 cells

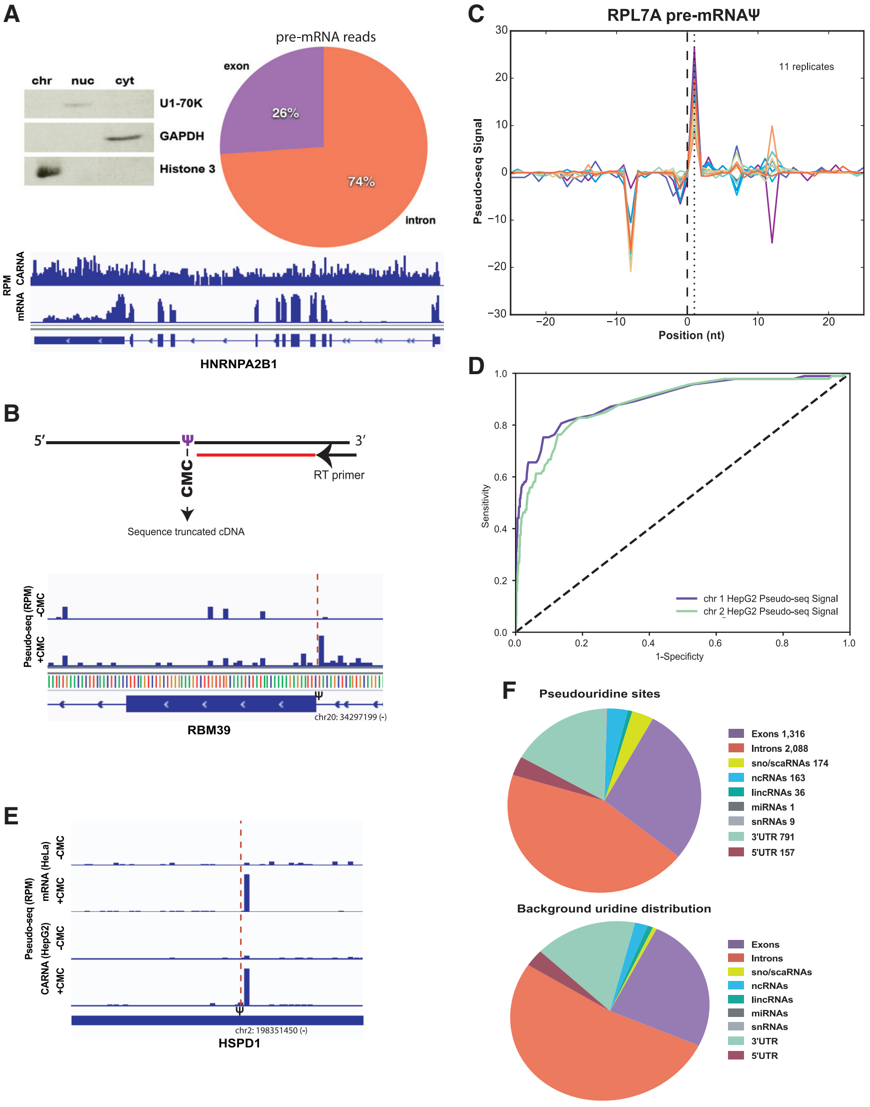

Figure 1. Pre-mRNA is pseudouridylated cotranscriptionally in human cells

(A) (Left panel) Western blot of HepG2 cellular fractions; equal cell volumes were loaded and probed with antibodies against GAPDH (cytoplasm), U1-70K (nucleoplasm), and Histone3 (chromatin). (Right panel) Distribution of pre-mRNA reads mapping to introns versus exons in the chromatin-associated RNA fraction. (Bottom panel) Genome browser view of reads per million mapping across the highly expressed gene *hnRNPA2B1* in a chromatin-associated RNA library compared with a poly(A)+ mRNA library from HepG2 cells.

(B) Detection of pseudouridine by Pseudo-seq with a representative genome browser view of Pseudo-seq reads mapping to RBM39; the red dotted line indicates the location of the pseudouridine (chr20:34297199) identified by a CMC-dependent reverse transcriptase stop 1 nt 3′ to the site. Reads per million (RPM).

(C) Pseudo-seq signal, equal to the difference in normalized reads between the +CMC and mock libraries. Traces for 11 biological replicates of chromatin-associated RPL7A pre-mRNA pseudouridine (chr9:136217792) are shown.

(D) ROC (Receiver Operating Characteristic) curve of true-positive versus false-positive rates of known pseudouridine locations in mature human rRNA for two representative chromatin-associated RNA replicates. The Pseudo-seq signal is displayed for both replicates.

(E) Representative genome browser view of Pseudo-seq reads mapping to HSPD1 from HepG2 chromatin-associated RNA and HeLa mRNA; the red dotted line indicates the location of this cell-type-conserved pseudouridine identified by a CMC-dependent reverse transcriptase stop 1 nt 3′ to the site.

(F) (Top panel) Summary of pseudouridines sites identified in chromatin-associated RNAs. (Bottom panel) Distribution of background uridines meeting the minimum read cutoff for site calling.

(Figure S1G), which is consistent with cell-type-specific mRNA pseudouridylation and/or with cytoplasmic mRNA modification.

Pseudouridines are enriched near alternative splice regions and splice sites

To explore the possibility of there being a role for pseudouridines in pre-mRNA processing, we investigated the location of pseudouridines relative to splicing features. We compared the fraction of called pseudouridines within splice sites (ss) (6 nt from exon ends) and in proximal introns (within 500 nt of ss) with the fraction of uridines meeting our coverage cutoffs for detection in these regions (Figure 2A). A hypergeometric test (Fisher's exact test) found that intronic pseudouridines are enriched compared with uridines within 6 nt of exon ends (p value < 0.55e−6). We also found that 752 pseudouridines are enriched in proximal introns within 500 nt of ss (p value = 1.3e−5) where splicing regulatory elements, such as intronic splicing enhancers and silencers, are often found (Figure 2A; Table S1C). Furthermore, we identified pseudouridines at 3′ (32) and 5′ (9) ss, polypyrimidine tracts (PPT) (72), and branch site regions (37) (Figure 2A). Pseudouridines occur at critical residues for splicing, including the conserved pyrimidine before the 3′ ss (YAG), in the region of the 5′ ss that base pairs with U1 snRNA, and in the branch site region that base pairs with U2 snRNA.

We further explored the potential for cotranscriptional pre-mRNA pseudouridylation to regulate splicing by determining the distribution of intronic pseudouridines with respect to alternatively spliced regions. We compared the distribution of called pseudouridines with uridines meeting our coverage cutoffs for detection in introns flanking alternatively spliced region categories (Figure 2B). Pseudouridines are notably enriched around alternative ss, including in the introns flanking cassette exons, introns of alternative 5′ and 3′ ss, and retained introns (RIs) (Figure 2B). By contrast, pseudouridines are depleted from the introns of constitutive and other exons (Figure 2B). The observed difference between the overall distribution of pseudouridines

Please cite this article in press as: Martinez et al., Pseudouridine synthases modify human pre-mRNA co-transcriptionally and affect pre-mRNA processing, Molecular Cell (2021), https://doi.org/10.1016/j.molcel.2021.12.023

and that of uridine in alternatively spliced regions was found to be statistically significant by a chi-squared test (p value = 2.2e−16). Together, the distribution of pseudouridines in alternatively spliced regions and near splice sites is consistent with the possibility of there being a role for pseudouridine in splicing regulation by pre-mRNA-modifying PUSs.

Site-specific pseudouridylation directly affects splicing *in vitro*

We site-specifically pseudouridylated pre-mRNA sequences (Figures 2C, 2D, and S2) to determine whether individual pseudouridines identified in cells are sufficient to directly affect pre-mRNA splicing *in vitro*. We generated chimeric two-exon pre-mRNA splicing reporters containing intronic PUS7 target sites in RBM39 and MDM2 through *in vitro* transcription, site-specifically pseudouridylated *in vitro* with recombinant PUS7, and isolated the modified pre-mRNA by purification (Figures S2A–S2C). Modified and unmodified control pre-mRNAs were incubated with wild-type (WT) nuclear extract under splicing conditions. Remarkably, a single endogenous intronic pseudouridine that was installed upstream of the 3′ ss in the RBM39 pre-mRNA was sufficient to directly enhance splicing as quantified by RT-PCR and compared with splicing of the unmodified control (Figures 2C and 2D). This effect of pseudouridine on splicing was observed in nuclear extracts from two different cell lines (Figures 2D and S2D) and across time points (Figure 2C). Similarly, modifying an MDM2 splicing reporter with a pseudouridine at an endogenously modified 3′ ss UAG enhanced splicing *in vitro* (Figures S2E and S2F). These results demonstrate a direct biochemical effect of individual endogenous pre-mRNA pseudouridines on splicing.

Pseudouridines are enriched in RBP binding sites

How might a single intronic pseudouridine alter the splicing outcome? Given that diverse RBPs show altered affinity for their target RNAs following artificial incorporation of pseudouridine (Chen et al., 2010; Delorimier et al., 2017; Vaidyanathan et al., 2017), we investigated the overlap of pre-mRNA pseudouridines with the binding sites of regulatory RBPs. We computationally compared pre-mRNA pseudouridines with RBP binding sites that were identified by enhanced UV crosslinking followed by immunoprecipitation and sequencing (eCLIP-seq) for 103 RBPs from HepG2 cells (Van Nostrand et al., 2016; Nussbacher and Yeo, 2018) (Figures 3A–3D). Binding sites for each examined RBP overlap tens to hundreds of pseudouridines as demonstrated by the eCLIP peaks with significant enrichment over the size-matched input (SMI) (>4-fold enrichment and adjusted p value < 0.001) (Figures 3A–3C). Strikingly, we found 5,359 significant eCLIP clusters (RBP binding sites) that overlap pseudouridines and 40% (1,922/4,789) of unique pseudouridines overlapped the validated RBP binding sites across the transcriptome, including 386 Ψ-RBP overlaps located in introns (Table S1E). Of these 386 Ψ-RBP overlaps, 249 are in introns flanking the annotated alternatively spliced exons.

We determined the statistical significance of pseudouridine co-localization within the binding sites for individual RBPs by comparing the fraction of eCLIP peaks that overlap pseudouridines with the expected overlap for sites that were randomly located (shuffled) within intronic regions (Figure 3D; Table S1F). *Z* scores were generated for each RBP by performing a thousand shuffles (Table S1F), revealing 33 RBPs with a *Z* score above 10 ($p < 10^{-5}$) (Figure 3D). As another control, to account for the possibility of the preferential detection of binding to abundant uridines, we performed the same experiment with all unmodified uridines that met the criteria for pseudouridine detection. The *Z* scores for pseudouridines and uridines overlapping the RBP binding sites for each RBP are provided in Table S1F and plotted for comparison (Figure 3E). All RBPs were underrepresented for intersection with unmodified uridines, except for U2AF2, which is known to bind a uridine-rich motif (Figure 3E). Thus, pseudouridines frequently occur within the binding sites for regulatory RBPs, and these features overlap more often than expected by chance.

Many of the highest scoring RBPs with binding sites that overlap intronic pseudouridines have documented roles in splicing regulation, including core splicing factors such as U2AF2, U2AF1, SF3A3, and PRPF8 (Figures 3A–3D; Table S1E). Other high-scoring RBPs include polyuridine and polypyrimidine-binding splicing factors such as hnRNP C, PTBP1, and TIA1 (Figure 3D; Table S1E). We observe an enrichment of polyuridine and polypyrimidine in the sequences flanking pseudouridines consistent with the enrichment of pseudouridine in the binding sites of RBPs (e.g., U2AF2) that are known to bind to these sequences (Figure S3B; Table S1F). These and other RBPs are known to be associated with nuclear RNAs and have diverse roles in RNA metabolism (Gratenstein et al., 2005; Pan et al., 2008; Fu and Ares, 2014; Zong et al., 2014; Attig et al., 2018). We also find pseudouridines enriched within pre-mRNAs encoding RBPs and splicing factors, suggesting another way by which pseudouridines might affect RBP activity (Figure S3C; Table S1G). Altogether, these results establish widespread co-occurrence of newly identified pre-mRNA pseudouridines at sites likely to affect splicing, including the binding sites of regulatory RBPs, in proximal introns of alternatively spliced regions, and at ss.

PUS1, RPUSD4, and PUS7 are predominant pre-mRNA modifying enzymes

Human cells, including HepG2, express up to 13 PUSs. To identify which enzymes target pre-mRNA and potentially regulate splicing, we took an *in vitro* approach. This strategy overcomes a critical limitation of cell-based endogenous pseudouridine assignment, which requires very deep sequencing of PUS-depleted cells to avoid false negatives and accurately interpret the absence of reads as evidence for the modification by the PUS in WT cells. The very large size of the human pre-mRNA transcriptome makes sequencing cellular RNA to sufficient depth unfeasible for our purpose. A recently developed high-throughput *in vitro* pseudouridylation assay (Carlile et al., 2019; Martinez and Gilbert, 2021) using purified PUS overcomes this limitation to identify which PUS(s) directly pseudouridylate sites of interest, including those in lowly expressed RNAs. We verified excellent agreement between genetic and *in vitro* assignment approaches by cross-validating 85% of yeast PUS1-dependent pseudouridine sites in mRNA (Carlile et al., 2014, 2019; Figure 4A). Although human PUS7 and TRUB1 recognize their targets in the context of a sequence motif, the features required

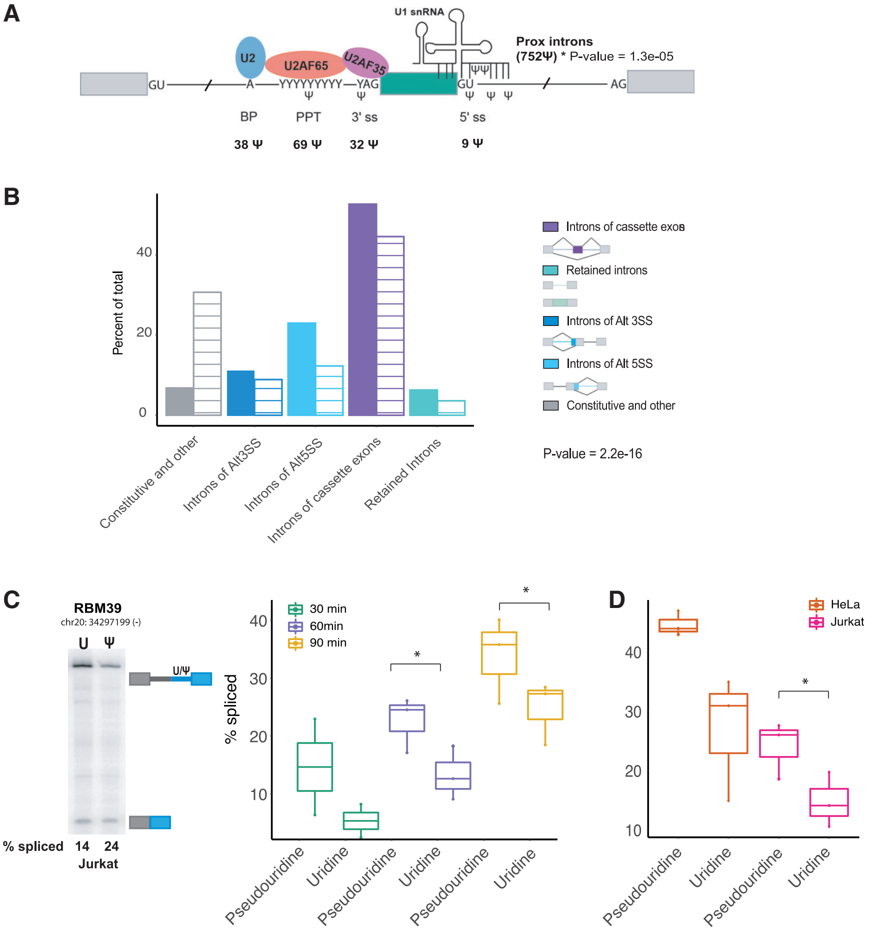

Figure 2. Pseudouridines are enriched around splicing regulatory features and directly affect splicing

(A) Schematic of a spliced exon including the core signals for splice-site recognition: branch point region (BP), polypyrimidine tract (PPT), and 5′ and 3′ splice-site (ss). The number of pseudouridines identified in each splice-site region is summarized below the schematic. Pseudouridines are enriched in proximal introns (within 500 nt) of splice sites, p value = 1.3e−5 from Fisher's exact test and within splice sites (within 6 nt from exoni ends), p value = 0.55e−6 from Fisher's exact test.

(B) Distribution of pseudouridines (filled bars) versus uridines with adequate read coverage in the introns (line bars) of the annotated alternatively spliced regions. p value = 2.2e−16 denotes a significant change in the distribution of pseudouridine relative to the uridine distribution as determined by chi-squared test for the overall change in proportions across regions. Alternative splice sites are referred to as Alt SS.

(C) Representative RT-PCR gel of *in vitro* splicing of RBM39 two-exon reporter (Figures S2A and S2C) that was either unmodified or site-specifically modified with pseudouridine (±Ψ) in splicing-competent WT Jurkat nuclear extract.

(D) Quantification of (percentage) the *in vitro* splicing of the RBM39 reporter in a splicing time course (30, 60, and 90 min) in Jurkat nuclear extract. Data are displayed as a stripchart with box plot, where the dots represent the value for each sample for a given condition (30 [n = 2], 60 [n = 3], and 90 min [n = 3]). p values were calculated by a paired t test, and difference considered significant if p value < 0.05. An asterisk denotes significance.

(E) Quantification of *in vitro* splicing of the RBM39 reporter that was either unmodified or site-specifically modified with pseudouridine (±Ψ) in Jurkat and HeLa nuclear extract. Quantification of percentage spliced from n = 3 is displayed as a stripchart with box plot, where the dots represent the value for each sample for a given cell type. p values were calculated by a paired t test, and the difference is considered significant if p value < 0.05. An asterisk denotes significance.

by the other 10 human PUS for targeting have not been characterized, making it difficult to predict the enzymes that direct the modification of identified sites in pre-mRNA.

To identify human PUSs that directly pseudouridylate pre-mRNA sequences, we synthesized a pool of RNA, containing each identified pseudouridine site flanked by 130 nt of endogenous sequence (Figure 4A). The resulting RNA pool was incubated in separate reactions with individual recombinant human pseudouridine synthases, including PUS1, PUS7, PUS7L, PUS10, RPUSD2, RPUSD4, TRUB1, TRUB2, or HepG2 nuclear extract; the pseudouridylation of the RNA from the pool was detected by Pseudo-seq. Pseudouridine sites were classified as direct targets of individual PUS using a statistically principled analysis pipeline (Martinez et al., 2021). This approach considers RT stops at the position of interest relative to surrounding positions, and the significance of a peak is determined relative to the positions surrounding it by means of a *Z* score calculation (STAR Methods). PUS-dependent pseudouridine sites are then identified as those that have a high *Z* score in the CMC-treated library and a low *Z* score in a no-PUS CMC-treated control library (Figure S4B). We identified hundreds of endogenous pre-mRNA pseudouridine sites as direct targets of one of the 8 tested PUSs (Figures 4B–4D and S4B–S4E; Table S1H). Importantly, the *in-vitro*-validated sites had a similar distribution across RNA features and classes as the total list of candidate pseudouridines identified in chromatin-associated RNA from cells (Figures 1F and 4C).

We identified PUS1, PUS7, and RPUSD4 as pre-mRNA pseudouridylating enzymes (Figure 4D). Orthologous yeast proteins Pus1 and Pus7 pseudouridylate the majority of known yeast mRNA sites (Carlile et al., 2014; Schwartz et al., 2014), suggesting a broad conservation of mRNA targeting by these PUS. RPUSD4 is a member of a PUS family that has expanded to include 4 paralogs in higher eukaryotes (chordates) and was not previously known to have mRNA targets. Importantly, PUS1, PUS7, and RPUSD4 are present in the nucleus in human cells (Fernandez-Vizarra et al., 2007; Stadler et al., 2013; Ji et al., 2015) where they have access to pre-mRNA. There is almost no redundancy among the *in vitro* targets of each PUS (Figures S4B–S4D), suggesting the presence of distinct targeting mechanisms and potentially specific regulatory programs. The fact

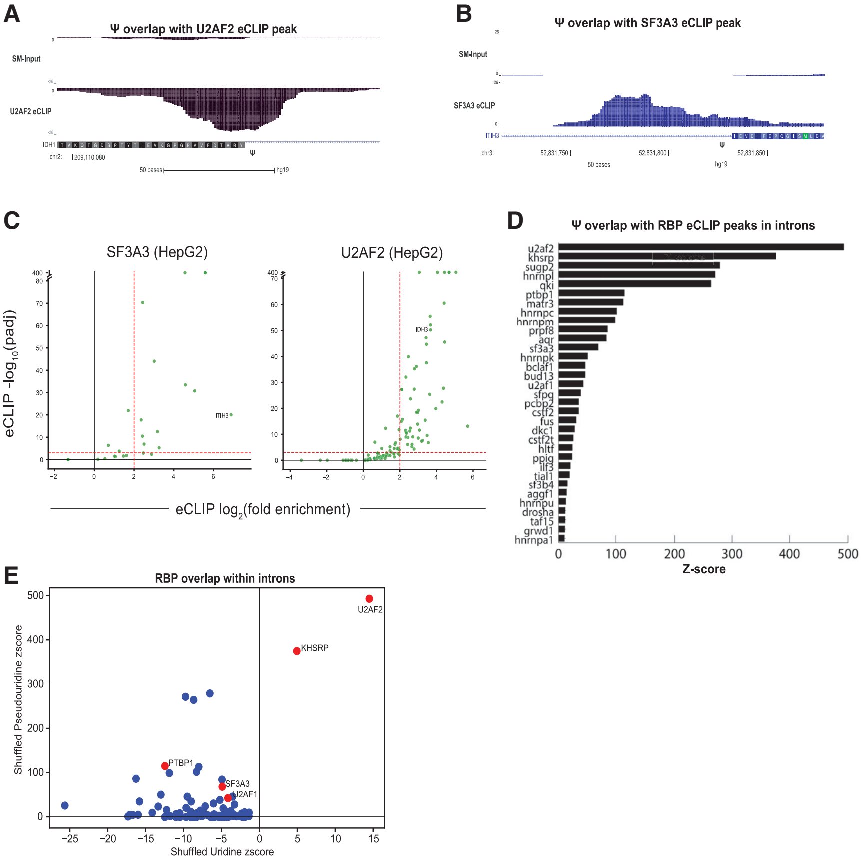

Figure 3. Pseudouridines are enriched in RNA-binding protein binding sites

(A and B) (A) Genome browser views of U2AF2 and (B) SF3A3 eCLIP peaks and size-matched input controls (SMI) on IDH1 and ITIH3, respectively. The location of pseudouridine relative to the eCLIP peak is denoted by (Ψ).

(C) Volcano plots of pseudouridines overlapping RBP eCLIP peaks displaying the fold enrichment (IP over size-matched input) versus the SMI-normalized adjusted p value (Van Nostrand et al., 2016). The overlap between eCLIP peaks and pseudouridines is shown for two RBPs, U2AF2 and SF3A3. Proximal introns refer to intronic sequences <500 nt from splice sites, and distal introns refer to intronic sequences >500 nt from splice sites.

(D) *Z* scores were generated by comparing the fraction of eCLIP peaks overlapping pseudouridines with the calculated overlap after shuffling pseudouridines within intronic regions 1,000 times.

(E) The *Z* score of pseudouridines shuffled 1,000 times within intronic regions plotted against the *Z* score of uridines shuffled 1,000 times within intronic regions.

that PUS1, RPUSD4, and PUS7 pseudouridylate the majority of identified pre-mRNA sites is consistent with their relatively high expression in HepG2 cells (Figures S4C–S4E). Some sites were pseudouridylated in nuclear extract but not by purified PUS, implying that at least one additional human PUS also pseudouridylates pre-mRNA and/or that some sites require cofactors that are supplied in the nuclear extract (Figure 4D; Table S1H). Although *in vitro* pseudouridylation allows for a confident assignment of successfully modified RNAs to specific PUS, there are many potential mechanisms producing false-negative results (see Discussion). Thus, some unassigned sites could still be the cellular targets of one of the tested PUS. These results identify site-specific RNA targets for previously uncharacterized PUS (e.g., RPUSD2, PUS7L) and substantially expand the known targets for others (e.g., PUS1, PUS7) to include pre-mRNAs.

Most PUS proteins pseudouridylate their targets in diverse sequence contexts and do not display strong sequence preferences (Figure S4F). This may reflect a predominantly structural mode of mRNA target recognition, as shown for yeast Pus1 (Carlile et al., 2019). By contrast, the targets of PUS7 are highly enriched for a UNΨAR motif, which is similar to, but a more permissive version of, the motif recognized by yeast Pus7 (Figure 4E). This motif also overlaps with the YAG of the 3′ ss for multiple PUS7 targets (Table S1H). The PUS7 motif is enriched among all chromatin-associated pseudouridines identified in HepG2 cells (Figure S4G), including some sites that are not modified by the recombinant protein *in vitro* (discussion). We identified comparatively few targets of the mRNA-targeting PUS, TRUB1 (Figure 4D), which occur primarily in the preferred TRUB1 sequence context GUΨCNANNC (Safra et al., 2017; Figure 4E). It is possible that TRUB1 targets were undercaptured because of the sequence bias in the ligation efficiency of circLigase (used for library preparation). Together, our *in vivo* pseudouridine profiling and *in vitro* PUS target validation identify pre-mRNA sites as the largest class of PUS targets and reveal the potential for multiple PUSs to influence pre-mRNA processing by pseudouridylating diverse nascent pre-mRNA sequences.

Pseudouridine synthases PUS1, RPUSD4, and PUS7 regulate alternative splicing

Taken together, the prevalence of pseudouridines in alternatively spliced pre-mRNAs (Figure 2A) and within splicing factor binding sites (Figures 3A–3D),our evidence that pseudouridine directly affects splicing *in vitro* (Figures 2C and 2D) and evidence from the literature that diverse RNA-RNA (Newby and Greenbaum, 2001; Hudson et al., 2013; Kierzek et al., 2014) and RNA-protein (Chen et al., 2010; Delorimier et al., 2017; Vaidyanathan et al., 2017) interactions are sensitive to pseudouridine, suggested that altering PUS activity could cause changes in splicing. PUS1, PUS7, and RPUSD4 emerged as likely candidates to influence splicing from our *in vitro* pre-mRNA pseudouridylation assay (Figure 4D). We first examined whether PUS1-dependent pseudouridylation influenced splicing by making PUS1 knockout (KO) HepG2 cells using CRISPR/Cas9 (Figure 5A). We obtained highly reproducible RNA-seq data from poly(A)+ mRNA from PUS1 KO and WT cells ($R^2 > 0.96$) and quantified differences in alternative splicing and mRNA abundance (STAR Methods). Strikingly, PUS1 KO leads to thousands of changes in alternative splicing, as defined by splicing events that were statistically significant (FDR < 0.05) and exhibited greater than 10% of difference in inclusion levels compared with WT cells (Figures 5A and 5B; Table S1I). Of these differential splicing changes, 195 exhibited a greater than 50% of difference in inclusion levels between conditions. These changes in splicing affected 1,617 genes and included cassette exons, alternative 5′ and 3′ ss, RI, and mutually exclusive exons (ME). We observed both differential inclusion and skipping of cassette exons upon PUS1 KO (Figures 5B, S5E, and S5F; Table S1I), showing that the effect of PUS1 on splicing is pre-mRNA-dependent. In contrast to these broad effects on alternative splicing, mature mRNA abundance changed very little, with approximately 100 mRNAs being significantly altered in cells lacking PUS1 (Figure S6A). Manual inspection of the affected mRNAs did not reveal any splicing factors or RBPs that would be expected to indirectly affect splicing (Table S1J).

We considered the possibility that the loss of site-specific pseudouridylation of U2 snRNA might underlie the splicing changes in PUS1 KO cells. In budding yeast, a single pseudouridine, Ψ44, in the U2 snRNA is installed by Pus1 (Massenet et al., 1999). However, the corresponding position in the human U2 snRNA, Ψ43, was not affected in PUS1 KO cells based on primer extension with U2-specific primers (Figure S6A). This result is consistent with a previous report showing PUS1-independent pseudouridylation of the homologous U2 snRNA site in mouse cells that lack PUS1 (Deryusheva and Gall, 2017) and with the computational and biochemical evidence that human snRNAs are modified by the snoRNA/scaRNA-dependent PUSs, DKC1 (Karijolich and Yu, 2010; Wu et al., 2011). Ψ43 is predicted to be modified by DKC1 in complex with scaRNA8 (Deryusheva and Gall, 2017). No other detected U2 snRNA pseudouridines were affected in PUS1 KO HepG2 cells (Figures S6A and S6B) or mouse cells (Deryusheva and Gall, 2017). Thus, a mechanism other than the loss of U2 snRNA pseudouridylation is responsible for the widespread PUS1-sensitive alternative splicing.

Consistent with the possibility of there being direct effects of PUS1-dependent pre-mRNA pseudouridylation on splicing, *in vitro*-validated PUS1 targets in cassette exons or flanking introns of PUM2, ARHGAP5, C14orf159, SNHG12, ANKRD10, and TANK showed differential splicing in PUS1 KO cells (Figures 5B, 5C, and S5C). Other unassigned pseudouridines that were identified in cells overlap PUS1-sensitive cassette exons or their flanking introns (Figure S5E). Some of these sites could be PUS1 targets that were not recapitulated *in vitro* because of the limitations of the *in vitro* pseudouridylation assay (see Discussion). Alternatively, their splicing may be affected indirectly by the absence of PUS1. Unfortunately, we were unable to interrogate pseudouridine status in cells for the vast majority of PUS1-sensitive cassette exons and flanking introns (Figures S5D and S5F; Table S1I). This blind spot arises because orders of magnitude fewer reads are sufficient to quantify alternative splicing in mature poly(A)+ mRNA compared with the coverage required for pre-mRNA pseudouridine discovery.

We used inducible shRNA expression to deplete the essential (Shalem et al., 2014; Wang et al., 2014) pre-mRNA pseudouridylating enzyme RPUSD4 and PUS7 to determine their impact on alternative splicing by RNA-seq. Replicate experiments were reproducible ($R^2 > 0.98$ and $R^2 > 0.94$). The partial depletion of RPUSD4 (60%) and PUS7 (90%) produced widespread effects on alternative splicing, including 817 RPUSD4-sensitive cassette exons in 696 genes and 190 PUS7-sensitive cassette exons in 175 genes (Figures 5A and 5D; Tables S1K and S1L). The RPUSD4 and PUS7 samples were sequenced at lower depth than the PUS1 KO cells, possibly contributing to fewer identified splicing changes. NAP1L4 is an example of a PUS7-sensitive alternatively spliced exon where PUS7 directly pseudouridylates a position near the exon, in the upstream intron (Figures 5D and 5E). As with PUS1, we lacked data for the pseudouridine status of most RPUSD4- and PUS7-sensitive exons in cells because of coverage limitations (Figures S5D and S5G). PUS7 depletion resulted in 374 differentially expressed genes (Figure S6B; Table S1M), consistent with previous studies showing altered PUS7-dependent mRNA levels in yeast (Schwartz et al., 2014). By contrast, RPUSD4 depletion resulted in almost no significant changes in mRNA levels (Figure S6C; Table S1N). As expected for shRNA-mediated depletion, PUS7 and RPUSD4 mRNAs were significantly downregulated (Figures S6B and S6C).

Each PUS pseudouridylates distinct pre-mRNA targets with little overlap (Figures 5F and S4C–S4E). Consistently, the depletion of each of the predominant pre-mRNA-targeting PUS produced distinct changes in the pattern of alternative splicing (Figure 5G). Notably, the pervasiveness and magnitude of PUS-dependent splicing changes are comparable to the effects of depleting canonical splicing regulators (Van Nostrand, 2018). These results support the presence of a widespread and nonredundant role for multiple PUSs in alternative splicing regulation. Given the enrichment of pseudouridines around alternatively spliced regions and our demonstration that endogenous pseudouridines can have direct biochemical effects on splicing *in vitro* (Figures 2B–2D and S2), we expect a subset of the splicing changes in PUS knockout/knockdown cells to be a consequence of direct pre-mRNA pseudouridylation. However, we cannot rule out that some of the PUS-sensitive events are an indirect consequence of the reduced pseudouridylation of other targets. Taken together, these findings support the premise that there is a broad potential for pre-mRNA pseudouridylation to impart widespread PUS-dependent alternative splicing.

Pseudouridine synthases PUS1, RPUSD4, and PUS7 regulate 3′ end processing

The finding that 3′ UTR pseudouridines are added to nascent pre-mRNA (Figure 1F) led us to hypothesize that pseudouridines might also influence another regulated step in pre-mRNA processing, namely, that of cleavage and polyadenylation. Therefore, we analyzed the RNA-seq data from PUS-depleted cells to find evidence of alternative cleavage and polyadenylation (APA) events. SRSF6 is an example of a shift toward usage of a proximal polyA site (PAS1) and the consequent expression of a shorter 3′ UTR isoform in the absence of PUS1 (Figure 6A). This pre-mRNA is directly modified by PUS1 at two locations near to and upstream of the proximal and the distal poly(A) sites (Table S1H). Overall, this analysis suggests that there are hundreds of instances of APA that exhibited reproducible and greater than 10% of differences in polyA site usage (PAU) in PUS-depleted cells compared with WT cells (Figure 6B; Tables

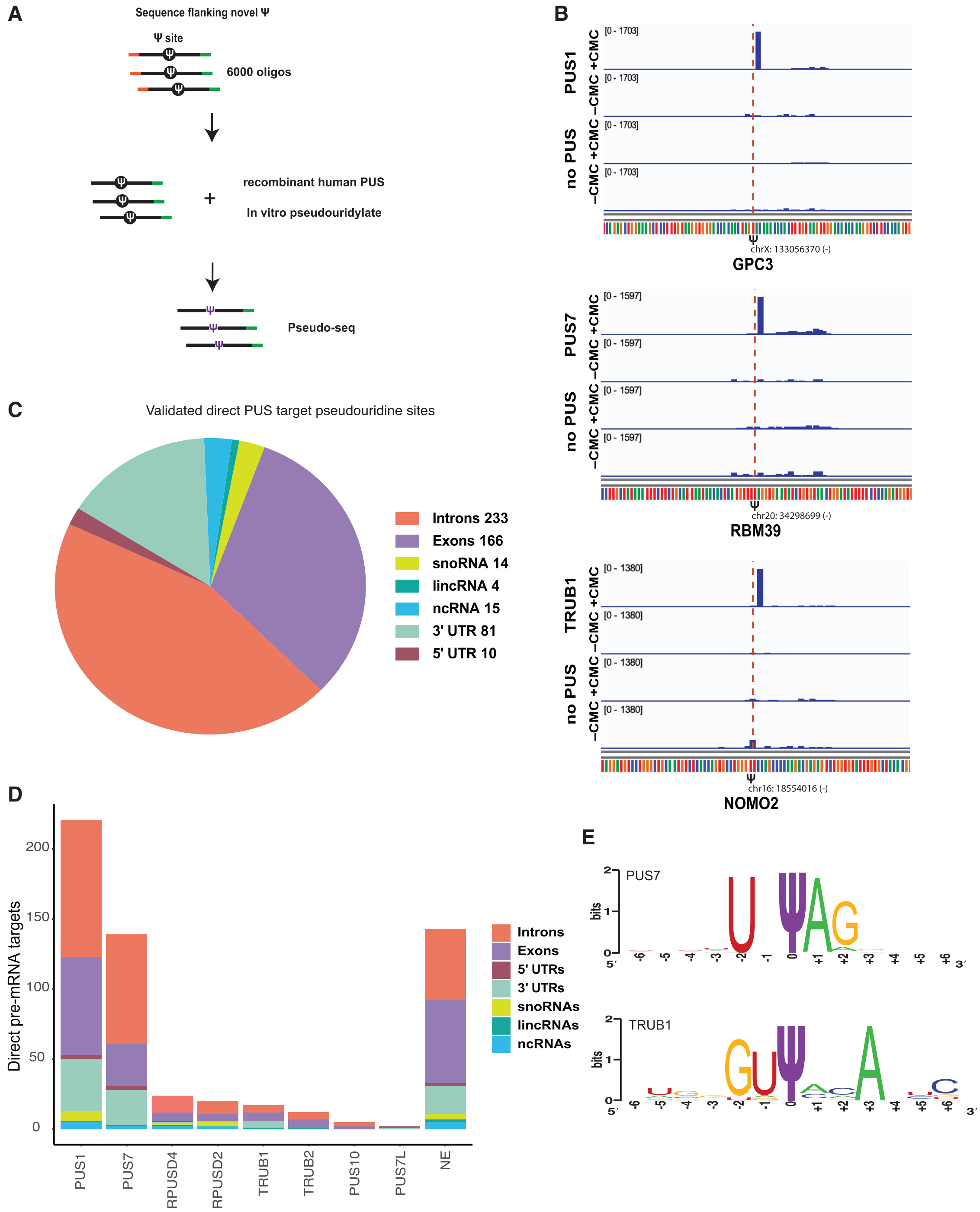

Figure 4. Multiple PUS pseudouridylate pre-mRNA sequences

(A) Schematic of *in vitro* pseudouridylation assay with RNA made from a pool of 6,000 oligos containing all the sites identified in HepG2 chromatin-associated RNA. *In vitro* pseudouridylation was carried out by incubating the pool RNA with recombinant human pseudouridine synthases (PUSs), and pseudouridines were identified by Pseudo-seq.

(B) Genome browser view of Pseudo-seq reads at pseudouridine sites after RNA incubation with a recombinant PUS or no-PUS control. Plots for three intronic pre-mRNA pseudouridines: a PUS1 target GPC3, PUS7 target in RBM39, and a TRUB1 target in NOMO2.

(C) Combined distribution of pseudouridines validated as direct targets of all tested PUS through *in vitro* Pseduo-seq assay.

(D) Summary of the pseudouridines assigned as direct targets of each PUS protein from *in vitro* Pseudo-seq assay.

(E) Sequence logo summarizing frequency of motifs identified among targets of PUS7 and TRUB1.

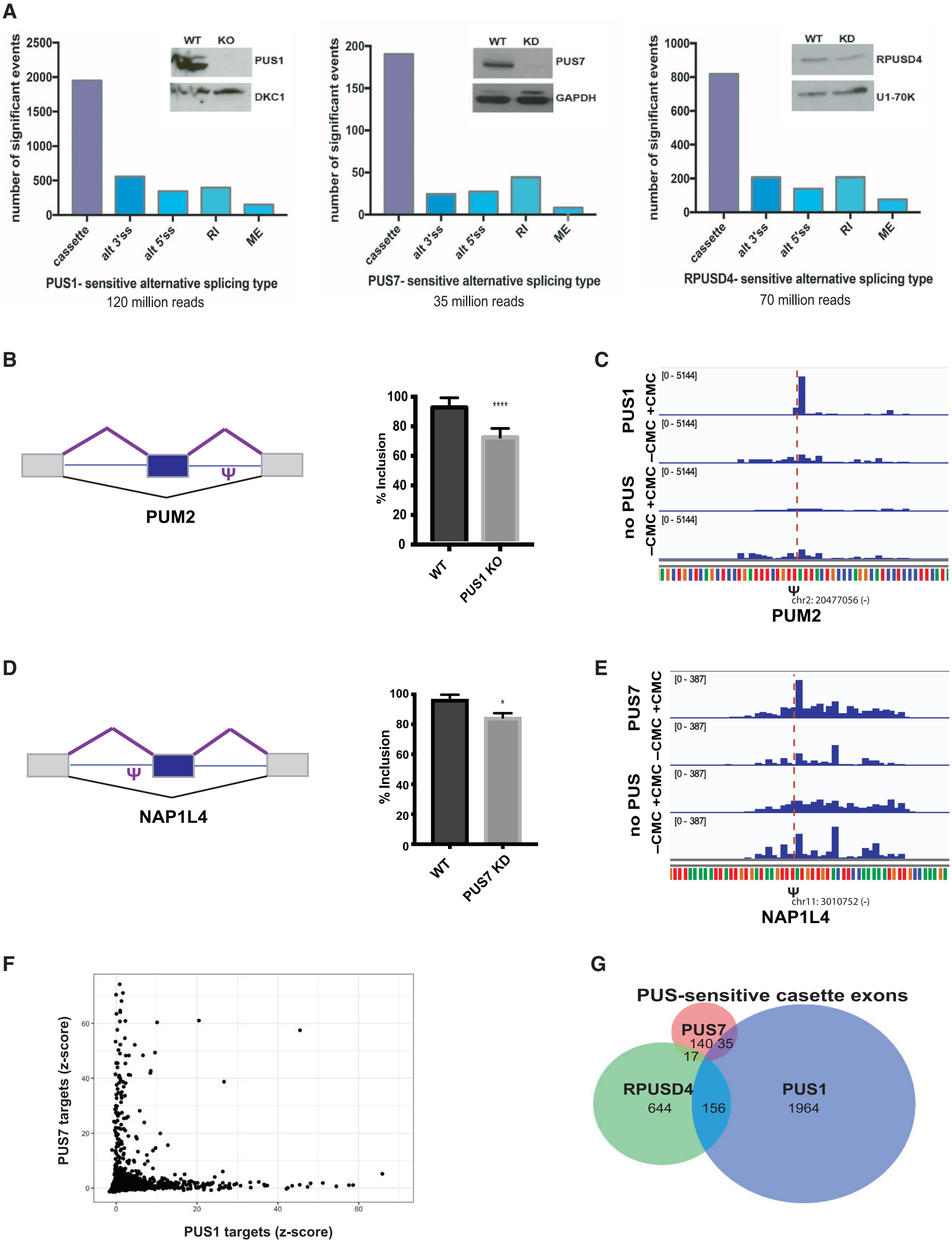

Figure 5. Pseudouridine synthases regulate alternative splicing

(A) (Left) Western blot of the CRISPR knockout PUS1 HepG2 cell line probed for PUS1 and a loading control. RNA was isolated from PUS1 knockout (KO) and wild-type (WT) cells, and mRNA-seq libraries were prepared from poly(A)+ mRNA. The number of significant alternative splicing changes in PUS1 KO versus WT (n = 2 biological replicates) is displayed by type of alternative splicing: cassette exons (cassette), alternative 3′ splice sites (alt 3′ss), alternative 5′ splice sites (alt 5′ ss), retained introns (RI), and ME. Significant alternative splicing events were determined from rMATS as those events that changed by greater than 10% of difference in percent inclusion and a false discovery rate (FDR) of ≤0.05. (Middle) Western blot of representative RPUSD4 knockdown (~60%) at 96 h after shRNA induction. RPUSD4-sensitive alternative splicing changes determined from RNA-seq analysis (n = 2 biological replicates) as above. (Right) Western blot of

(legend continued on next page)

S1O–S1Q). Applying 3′ end sequencing methods to PUS-depleted cells will facilitate the quantification of the full extent of PUS-dependent APA and allow for a precise annotation of the 3′ ends of affected transcripts in the future. However, many studies have used conventional RNA-seq data to infer changes in APA (Xia et al., 2014; Kim et al., 2015; Grassi et al., 2016; Ha et al., 2018; Goering et al., 2021), and in cases were the quantification of APA from conventional RNA-seq has been compared with 3′ end sequencing, strong correlations have been observed (Ha et al., 2018; Goering et al., 2021). Pre-mRNA pseudouridines were enriched in the binding sites of canonical cleavage and polyadenylation factors, CSTF2T and CSTF2, and in the binding sites of several RBPs known to regulate 3′ end processing (Figures 3D and 6C; Table S1E), suggesting a mechanism that could mediate altered 3′ end processing in response to PUS activity. These results extend the known roles of nuclear PUS to include controlling alternative 3′ end processing in human cells. The installation of pseudouridine cotranscriptionally positions it to influence multiple steps of pre-mRNA processing to establish distinct gene expression programs.

DISCUSSION

Mature human mRNAs were previously shown to be pseudouridylated, but the timing of pseudouridylation and the role of this modification in mRNA metabolism and gene regulation remained unaddressed. Here, by investigating chromatin-associated RNA, we uncovered a widespread modification of nascent pre-mRNA with pseudouridine, positioning pseudouridine to influence virtually all steps of mRNA processing. Consistent with this broad potential, we observed widespread changes in alternative splicing and 3′ end processing in response to changes in the expression of specific pre-mRNA-modifying PUSs. In further support of the function of pre-mRNA pseudouridines, we show that site-specific pre-mRNA pseudouridylation is sufficient to alter splicing outcomes *in vitro*. Notably, we find that pre-mRNA pseudouridines are significantly enriched within the experimentally determined binding sites of multiple splicing and processing factors and other regulatory RBPs. In light of the previous reports that the presence of pseudouridine changes the affinity of diverse RBPs for their target RNAs, this finding suggests a likely mechanism for pre-mRNA pseudouridylation to affect nuclear RNA processing. We note that pre-mRNA pseudouridylation is likely to be substantially more extensive than the sites identified here because stringent coverage criteria for detection and the large size of the nascent transcriptome restricted the pseudouridine discovery to ~1% of highly expressed genes.

We validated hundreds of candidate pseudouridines identified in cells as direct targets of one of 8 purified human PUS proteins tested *in vitro*. These results establish PUS1, PUS7, and RPUSD4 as pre-mRNA-modifying enzymes and add pre-mRNA as a new class of RNA targets for each of the tested PUS enzymes. Our data suggest that additional human PUS, among the 5 not tested here, modify pre-mRNA sites. Alternatively, some of the tested PUS may modify sites that were not recapitulated in our minimal *in vitro* system. Failure to be pseudouridylated *in vitro* could reflect the need for additional RNA sequences, cellular cofactors, low activity of recombinant protein, absence of protein modifications in recombinant protein, or other features present in the endogenous context such as co-transcriptional PUS recruitment. Although the PUS that modify the remaining candidate pseudouridine sites remain to be identified, unassigned sites resemble the *in vitro*-validated sites in Pseudo-seq signal intensity and reproducibility in cells (Figures 1C and 1E; Table S1C), suggesting that we have validated only a subset of true pseudouridine sites. Future work will likely reveal which of the other human PUS pseudouridylate pre-mRNA sequences and whether cofactors or cotranscriptional PUS recruitment are required for the installation of some pseudouridines.

About half of the newly identified candidate pseudouridines are located in introns, where pseudouridine was not previously known to occur. These pseudouridines are well positioned to affect alternative splicing because of their enrichment in proximal introns, alternatively spliced regions, and within splicing factor binding sites. Consistent with this regulatory potential, we find that the installation of a single intronic pseudouridine is sufficient to affect the splicing outcome *in vitro*. An advantage of these *in vitro* experiments is the avoidance of all potentially confounding indirect effects of the genetic manipulation of PUS activity in cells, providing strong support for a direct mechanistic effect of individual endogenous pre-mRNA pseudouridines on splicing.

Notably, the expression levels of the PUS proteins vary across tissues and cell types (Figures S7A–S7C), highlighting the regulatory potential for pre-mRNA pseudouridylation by these factors to control human gene expression. In support of this idea, we present evidence for the cell-type-specific regulation of pre-mRNA pseudouridylation in HepG2 compared with that in HeLa (Figure S1G) and show that the genetic manipulation of pre-mRNA-pseudouridylating enzymes PUS1, PUS7, and RPUSD4 in cells leads to thousands of changes in alternative

representative PUS7 knockdown (~90%) at 96 h after shRNA induction. PUS7-sensitive alternative splicing changes determined from RNA-seq analysis (n = 3 biological replicates) as above.

(B) (Left) Schematic of a cassette exon in PUM2 and location of pseudouridine. (Right) Quantification of exon inclusion in WT and PUS1 KO based on junction spanning reads from RNA-seq. Asterisk denotes statistical significance based on p value < 0.05 as calculated by rMATS.

(C) Genome browser view of Pseudo-seq reads of the intronic PUM2 pseudouridine site (Figure 5B) after pseudouridylation with recombinant PUS1 or in the absence of PUS.

(D) (Left) Schematic of a cassette exon in NAP1L4 and location of pseudouridine. (Right) Quantification of exon inclusion in WT and PUS7 KD based on junction spanning reads from RNA-seq. Asterisk denotes statistical significance based on p value < 0.05 as calculated by rMATS.

(E) Genome browser view of Pseudo-seq reads of the intronic NAP1L4 pseudouridine site (Figure 5D) after pseudouridylation with recombinant PUS7 or in the absence of PUS.

(F) Scatter plot showing pairwise comparisons of *Z* score values at candidate pseudouridine sites incubated with recombinant PUS1 versus PUS7.

(G) Venn diagram of overlap among cassette exons regulated by PUS1, PUS7, and RPUSD4.

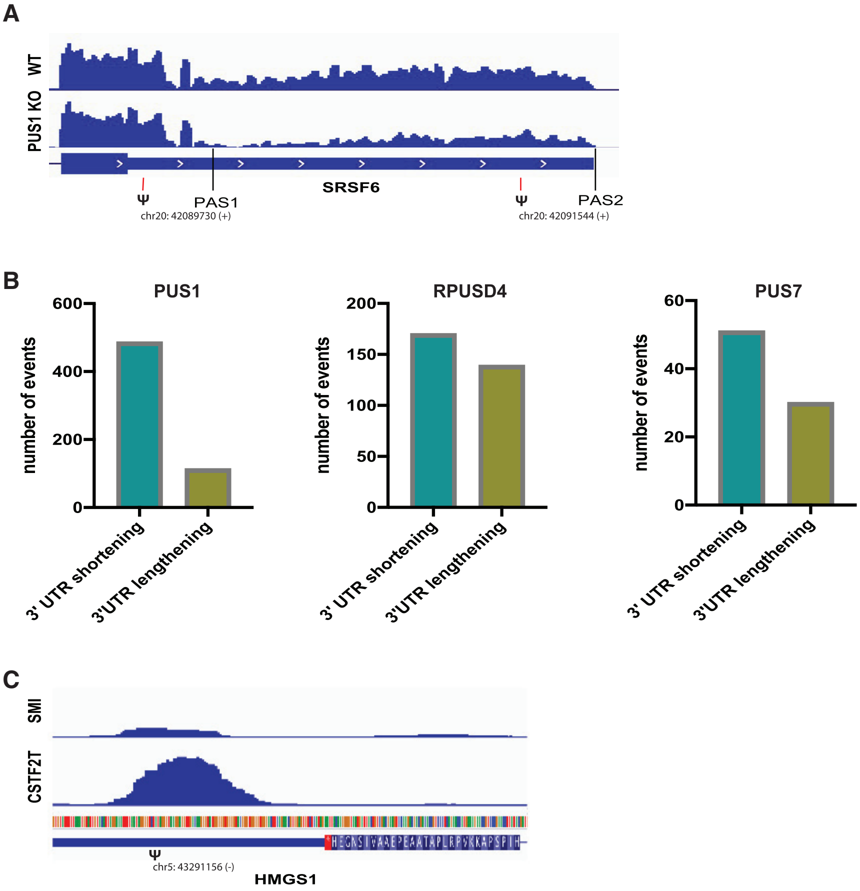

Figure 6. Pseudouridine synthases regulate 3′ end processing

(A) Genome browser view of a PUS1-dependent alternative cleavage and polyadenylation (APA) event in the 3′ UTR of SRSF6. Upon PUS1 KO, there is a shift toward the usage of a proximal polyA site (PAS1) and away from the diatal polyA site (PAS2), resulting in the expression of a shorter 3′ UTR isoform. The location of a two pseudouridine in this 3′ UTR upstream of each PAS is indicated.

(B) The number of significant alternative cleavage and polyadenylation events in PUS1 KO (n = 2 biological replicates), RPUSD4 KD (n = 2 biological replicates), or PUS7 KD (n = 3 biological replicates) compared with WT is displayed by the type of APA: 3′ UTR shortening and 3′ UTR lengthening. Significant APA events were determined from QAPA as those events that changed by greater than 10% of difference in polyA site usage and were reproducible across replicates.

(C) Genome browser views of CSTF2T eCLIP peak and size-matched input controls (SMI) in the 3′ UTR of HMGS1. The location of a pseudouridine relative to the eCLIP peak is denoted by Ψ.

splicing and APA that altered the 3′ UTR length for hundreds of mRNAs. The mechanisms guiding cell-type-specific pre-mRNA modification and their functional outcome on cell-type-specific gene regulation are open areas for investigation.

Mechanistically, pseudouridines in pre-mRNA have the potential to influence splicing by three main mechanisms: altering pre-mRNA-snRNA interactions, modulating pre-mRNA-protein interactions, or by influencing the pre-mRNA secondary structure (Martinez and Gilbert, 2018). We identified pseudouridines in the regions poised to function by any of these modes. Single pseudouridines stabilize synthetic RNA duplexes by 1–2 kcal/mol compared with uridine base pairs (Hudson et al., 2013; Kierzek et al., 2014). This stabilizing effect is predicted to enhance splice-site recognition by promoting the binding of spliceosomal snRNAs to the pseudouridylated 5′ ss or branch site. Pseudouridines have also been shown to alter the affinities of various RBPs (e.g., PUM2, MBNL1, U2AF2) for RNA *in vitro* (Chen et al., 2010; Delorimier et al., 2017; Vaidyanathan et al., 2017). We identify 3′ ss recognition factor U2AF2 as one of the factors that has a significant overlap between its binding sites and pseudouridine locations in pre-mRNA. U2AF1, the other component of the U2AF heterodimer, also overlaps pseudouridines locations in pre-mRNA, including at the 3′ ss. The sensitivity of most RBPs to the pseudouridylation of their binding sites remains to be determined, but many are likely to be affected given that diverse RBPs show 2- to 100-fold differences in the affinity for artificially pseudouridylated compared with unmodified RNA (Chen et al., 2010; Delorimier et al., 2017; Vaidyanathan et al., 2017). Finally, pseudouridylation could indirectly alter ss accessibility and/or splicing factor binding by changing the pre-mRNA secondary structure, as has recently been demonstrated for certain intronic m6A modification sites (Liu et al., 2015).

Altogether, our results implicate pseudouridine and the pre-mRNA-modifying PUS as novel regulators of pre-mRNA processing. This may have clinical relevance for the multiple PUS implicated in mitochondrial myopathy (Bykhovskaya et al., 2004; Fernandez-Vizarra et al., 2007), digestive disorders (Barrett et al., 2008; Dubois et al., 2010; McGovern et al., 2010; Festen et al., 2011; Repnik and Potočnik, 2016), intellectual disability (Shaheen et al., 2016; de Brouwer et al., 2018), resistance to viral infection (Marceau et al., 2016; Zhao et al., 2016), X-linked dyskeratosis congenita (Heiss et al., 1998; Knight et al., 1999), and cancer (Mannoor et al., 2012; Williams and Farzaneh, 2012; Thorenoor and Slaby, 2015; McMahon et al., 2015).

Limitations of the study

Our study reveals that pre-mRNAs are extensively pseudouridylated cotranscriptionally, which positions pseudouridine to influence any step of mRNA processing. We recognize that this represents a subset of true sites as this approach is limited to highly expressed genes that were detected with sufficient coverage by the pseudouridine profiling of chromatin-associated RNA. Therefore, the lack of evidence for the presence of pseudouridylation cannot be interpreted as lack of pseudouridylation. This limitation also prevented us from investigating the pseudouridine status of many PUS-dependent pre-mRNA processing changes. Alternative methods for pseudouridine detection, such as SCARLET (Liu and Pan, 2016), could be useful for the additional validation of candidate pseudouridines in pre-mRNA through an orthogonal method and for estimating stoichiometry at sites of interest.

We found a new role for PUS in regulating widespread pre-mRNA processing and presented evidence that pseudouridines can have a direct biochemical effect on splicing. However, we cannot rule out that some of the identified PUS-sensitive alternative splicing events are an indirect consequence of chronic PUS depletion. Additionally, our data suggest that PUS regulate 3′ end processing. Future characterization and quantification of exact mRNA 3′ ends through 3′ end sequencing will be valuable for further study of PUS-dependent APA regulation because the variability in the capture of mRNA 3′ ends in standard RNA-seq limits its application.

Finally, we show that multiple PUS directly modify pre-mRNA sequences in high-throughput *in vitro* pseudouridylation assays. This work demonstrates a new class of targets for many PUS that are associated with diseases and whose expression is regulated in different cell types. We caution that a negative result in this assay should not be interpreted strongly since failure to be pseudouridylated in this approach could also result from the need for additional RNA sequences, the absence of cellular cofactors, low activity of recombinant protein, protein modifications that are not present in recombinant protein, or other features present in the endogenous context such as cotranscriptional PUS recruitment.

STAR★METHODS

Detailed methods are provided in the online version of this paper and include the following:

- KEY RESOURCES TABLE
- RESOURCE AVAILABILITY
  - ○ Lead contact
  - ○ Materials availability
  - ○ Data and code availability
- EXPERIMENTAL MODEL AND SUBJECT DETAILS
  - ○ Cell culture
- METHOD DETAILS
  - ○ Total RNA Isolation
  - ○ Western Blotting
  - ○ CRISPR knockout generation
  - ○ PUS protein depletion
  - ○ Nuclear extract preparation
  - ○ Cellular Fractionation
  - ○ rRNA depletion
  - ○ Recombinant PUS plasmids and purification
  - ○ In vitro pseudouridylation
  - ○ Pseudo-seq
  - ○ RNA-seq
  - ○ Sequencing Analysis
  - ○ PUS protein assignment
  - ○ Alternative splicing analysis
  - ○ Differential gene expression analysis
  - ○ Enrichment analysis
  - ○ Motif enrichment
  - ○ GO analysis
  - ○ Analysis of RBP eCLIP overlap with pseudouridines
  - ○ *In vitro* splicing from nuclear extracts
  - ○ Site lists and reproducibility analyses
  - ○ Sequence context analyses
  - ○ RBS-Seq signal analysis
  - ○ Alternative cleavage and polyadenylation analysis
  - ○ Primer extension
- QUANTIFICATION AND STATISTICAL ANALYSIS

SUPPLEMENTAL INFORMATION

Supplemental information can be found online at https://doi.org/10.1016/j.molcel.2021.12.023.

ACKNOWLEDGMENTS

We thank Brenton R. Graveley for HepG2 cells, Tristan A. Bell for purified hPUS1, and Matthew G. Thompson and Kristen W. Lynch for splicing competent nuclear extracts and splicing reporter backbone plasmids. We thank Karla M. Neugebauer and members of the Gilbert Lab for helpful discussions and critical reading of the manuscript. This work was supported by NIH GM101316 and American Cancer Society RSG-13-396-01-RMC to W.V.G.; NIH HG004659 and HG009889 to G.W.Y.; and Jane Coffin Childs Postdoctoral Fellowship 161624T and NIH K99 GM135537 to N.M.M.

AUTHOR CONTRIBUTIONS

N.M.M. and W.V.G. conceived the project and designed experiments. A.S. purified recombinant proteins. C.S. performed bioinformatic analysis of HeLa mRNA sites from previous studies. J.K.N., M.C.B, S.S., and G.W.Y. designed and performed bioinformatic analysis of RBP binding sites. N.M.M. performed all other experiments and analysis. N.M.M. and W.V.G. wrote the manuscript with input from all authors.

DECLARATION OF INTERESTS

G.W.Y. is the cofounder of, a member of the Board of Directors of, on the scientific advisory board of, an equity holder in, and a paid consultant for Locanabio and Eclipse BioInnovations. G.W.Y. is a visiting professor at the National University of Singapore. G.W.Y.'s interests have been reviewed and approved by the University of California, San Diego, in accordance with its conflict of interest policies. The authors declare no other competing financial interests.

Received: September 2, 2021
Revised: November 4, 2021
Accepted: December 17, 2021
Published: January 19, 2022

REFERENCES

Anders, S., Pyl, P.T., and Huber, W. (2015). HTSeq–a Python framework to work with high-throughput sequencing data. Bioinformatics *31*, 166–169. https://doi.org/10.1093/bioinformatics/btu638.

Attig, J., Agostini, F., Gooding, C., Chakrabarti, A.M., Singh, A., Haberman, N., Zagalak, J.A., Emmett, W., Smith, C.W.J., Luscombe, N.M., and Ule, J. (2018). Heteromeric RNP assembly at LINEs controls lineage-specific RNA processing. Cell *174*, 1067–1081.e17. https://doi.org/10.1016/j.cell.2018.07.001.

Bailey, T.L., Johnson, J., Grant, C.E., and Noble, W.S. (2015). The MEME suite. Nucleic Acids Res *43*, W39–W49. https://doi.org/10.1093/nar/gkv416.

Barrett, J.C., Hansoul, S., Nicolae, D.L., Cho, J.H., Duerr, R.H., Rioux, J.D., Brant, S.R., Silverberg, M.S., Taylor, K.D., Barmada, M.M., et al. (2008).

Genome-wide association defines more than 30 distinct susceptibility loci for Crohn's disease. Nat. Genet. *40*, 955–962. https://doi.org/10.1038/ng.175.

Bhatt, D.M., Pandya-Jones, A., Tong, A.J., Barozzi, I., Lissner, M.M., Natoli, G., Black, D.L., and Smale, S.T. (2012). Transcript dynamics of proinflammatory genes revealed by sequence analysis of subcellular RNA fractions. Cell *150*, 279–290. https://doi.org/10.1016/j.cell.2012.05.043.

Birkedal, U., Christensen-Dalsgaard, M., Krogh, N., Sabarinathan, R., Gorodkin, J., and Nielsen, H. (2015). Profiling of ribose methylations in RNA by high-throughput sequencing. Angew. Chem. Int. Ed. Engl. *54*, 451–455. https://doi.org/10.1002/anie.201408362.

Bykhovskaya, Y., Casas, K., Mengesha, E., Inbal, A., and Fischel-Ghodsian, N. (2004). Missense mutation in pseudouridine synthase 1 (PUS1) causes mitochondrial myopathy and sideroblastic anemia (MLASA). Am. J. Hum. Genet. *74*, 1303–1308. https://doi.org/10.1086/421530.

Carlile, T.M., Martinez, N.M., Schaening, C., Su, A., Bell, T.A., Zinshteyn, B., and Gilbert, W.V. (2019). mRNA structure determines modification by pseudouridine synthase 1. Nat. Chem. Biol. *15*, 966–974. https://doi.org/10.1038/s41589-019-0353-z.

Carlile, T.M., Rojas-Duran, M.F., and Gilbert, W.V. (2015). Pseudo-seq: genome-wide detection of pseudouridine modifications in RNA. Methods Enzymol *560*, 219–245. https://doi.org/10.1016/bs.mie.2015.03.011.

Carlile, T.M., Rojas-Duran, M.F., Zinshteyn, B., Shin, H., Bartoli, K.M., and Gilbert, W.V. (2014). Pseudouridine profiling reveals regulated mRNA pseudouridylation in yeast and human cells. Nature *515*, 143–146. https://doi.org/10.1038/nature13802.

Chen, C., Zhao, X., Kierzek, R., and Yu, Y.T. (2010). A flexible RNA backbone within the polypyrimidine tract is required for U2AF65 binding and pre-mRNA splicing *in vivo*. Mol. Cell. Biol. *30*, 4108–4119. https://doi.org/10.1128/MCB.00531-10.

Czudnochowski, N., Wang, A.L., Finer-Moore, J., and Stroud, R.M. (2013). In human pseudouridine synthase 1 (hPus1), a C-terminal helical insert blocks tRNA from binding in the same orientation as in the Pus1 bacterial homologue TruA, consistent with their different target selectivities. J. Mol. Biol. *425*, 3875–3887. https://doi.org/10.1016/j.jmb.2013.05.014.

de Brouwer, A.P.M., Abou Jamra, R., Körtel, N., Soyris, C., Polla, D.L., Safra, M., Zisso, A., Powell, C.A., Rebelo-Guiomar, P., Dinges, N., et al. (2018). Variants in PUS7 cause intellectual disability with speech delay, microcephaly, short stature, and aggressive behavior. Am. J. Hum. Genet. *103*, 1045–1052. https://doi.org/10.1016/j.ajhg.2018.10.026.

deLorimier, E., Hinman, M.N., Copperman, J., Datta, K., Guenza, M., and Berglund, J.A. (2017). Pseudouridine modification inhibits muscleblind-like 1 (MBNL1) binding to CCUG repeats and minimally structured RNA through reduced RNA flexibility. J. Biol. Chem. *292*, 4350–4357. https://doi.org/10.1074/jbc.M116.770768.

Deryusheva, S., and Gall, J.G. (2017). Dual nature of pseudouridylation in U2 snRNA: Pus1p-dependent and Pus1p-independent activities in yeasts and higher eukaryotes. RNA *23*, 1060–1067. https://doi.org/10.1261/rna.061226.117.

Dobin, A., Davis, C.A., Schlesinger, F., Drenkow, J., Zaleski, C., Jha, S., Batut, P., Chaisson, M., and Gingeras, T.R. (2013). STAR: ultrafast universal RNA-seq aligner. Bioinformatics *29*, 15–21. https://doi.org/10.1093/bioinformatics/bts635.

Dubois, P.C.A., Trynka, G., Franke, L., Hunt, K.A., Romanos, J., Curtotti, A., Zhernakova, A., Heap, G.A., Adány, R., Aromaa, A., et al. (2010). Multiple common variants for celiac disease influencing immune gene expression. Nat. Genet. *42*, 295–302. https://doi.org/10.1038/ng.543.

Fernandez-Vizarra, E., Berardinelli, A., Valente, L., Tiranti, V., and Zeviani, M. (2007). Nonsense mutation in pseudouridylate synthase 1 (PUS1) in two brothers affected by myopathy, lactic acidosis and sideroblastic anaemia (MLASA). J. Med. Genet. *44*, 173–180. https://doi.org/10.1136/jmg.2006.045252.

Festen, E.A.M., Goyette, P., Green, T., Boucher, G., Beauchamp, C., Trynka, G., Dubois, P.C., Lagacé, C., Stokkers, P.C., Hommes, D.W., et al. (2011). A meta-analysis of genome-wide association scans identifies IL18RAP, PTPN2, TAGAP, and PUS10 as shared risk loci for Crohn's disease and celiac disease. PLoS Genet *7*, e1001283. https://doi.org/10.1371/journal.pgen.1001283.

Fu, X.D., and Ares, M. (2014). Context-dependent control of alternative splicing by RNA-binding proteins. Nat. Rev. Genet. *15*, 689–701. https://doi.org/10.1038/nrg3778.

Gilbert, W.V., Bell, T.A., and Schaening, C. (2016). Messenger RNA modifications: form, distribution, and function. Science *352*, 1408–1412. https://doi.org/10.1126/science.aad8711.

Goering, R., Engel, K.L., Gillen, A.E., Fong, N., Bentley, D.L., and Taliaferro, J.M. (2021). LABRAT reveals association of alternative polyadenylation with transcript localization, RNA binding protein expression, transcription speed, and cancer survival. BMC Genomics *22*, 476. https://doi.org/10.1186/s12864-021-07781-1.

Grassi, E., Mariella, E., Lembo, A., Molineris, I., and Provero, P. (2016). Roar: detecting alternative polyadenylation with standard mRNA sequencing libraries. BMC Bioinformatics *17*, 423. https://doi.org/10.1186/s12859-016-1254-8.

Gratenstein, K., Heggestad, A.D., Fortun, J., Notterpek, L., Pestov, D.G., and Fletcher, B.S. (2005). The WD-repeat protein GRWD1: potential roles in myeloid differentiation and ribosome biogenesis. Genomics *85*, 762–773. https://doi.org/10.1016/j.ygeno.2005.02.010.

Ha, K.C.H., Blencowe, B.J., and Morris, Q. (2018). QAPA: a new method for the systematic analysis of alternative polyadenylation from RNA-seq data. Genome Biol *19*, 45. https://doi.org/10.1186/s13059-018-1414-4.

Heiss, N.S., Knight, S.W., Vulliamy, T.J., Klauck, S.M., Wiemann, S., Mason, P.J., Poustka, A., and Dokal, I. (1998). X-linked dyskeratosis congenita is caused by mutations in a highly conserved gene with putative nucleolar functions. Nat. Genet. *19*, 32–38. https://doi.org/10.1038/ng0598-32.

Hudson, G.A., Bloomingdale, R.J., and Znosko, B.M. (2013). Thermodynamic contribution and nearest-neighbor parameters of pseudouridine-adenosine base pairs in oligoribonucleotides. RNA *19*, 1474–1482. https://doi.org/10.1261/rna.039610.113.

Huh, W.K., Falvo, J.V., Gerke, L.C., Carroll, A.S., Howson, R.W., Weissman, J.S., and O'Shea, E.K. (2003). Global analysis of protein localization in budding yeast. Nature *425*, 686–691. https://doi.org/10.1038/nature02026.

Ji, X., Dadon, D.B., Abraham, B.J., Lee, T.I., Jaenisch, R., Bradner, J.E., and Young, R.A. (2015). Chromatin proteomic profiling reveals novel proteins associated with histone-marked genomic regions. Proc. Natl. Acad. Sci. USA *112*, 3841–3846. https://doi.org/10.1073/pnas.1502971112.

Karijolich, J., and Yu, Y.T. (2010). Spliceosomal snRNA modifications and their function. RNA Biol *7*, 192–204. https://doi.org/10.4161/rna.7.2.11207.

Ke, S., Pandya-Jones, A., Saito, Y., Fak, J.J., Vågbø, C.B., Geula, S., Hanna, J.H., Black, D.L., Darnell, J.E., and Darnell, R.B. (2017). m6A mRNA modifications are deposited in nascent pre-mRNA and are not required for splicing but do specify cytoplasmic turnover. Genes Dev *31*, 990–1006. https://doi.org/10.1101/gad.301036.117.

Khoddami, V., and Cairns, B.R. (2013). Identification of direct targets and modified bases of RNA cytosine methyltransferases. Nat. Biotechnol. *31*, 458–464. https://doi.org/10.1038/nbt.2566.

Khoddami, V., Yerra, A., Mosbruger, T.L., Fleming, A.M., Burrows, C.J., and Cairns, B.R. (2019). Transcriptome-wide profiling of multiple RNA modifications simultaneously at single-base resolution. Proc. Natl. Acad. Sci. USA *116*, 6784–6789. https://doi.org/10.1073/pnas.1817334116.

Khodor, Y.L., Rodriguez, J., Abruzzi, K.C., Tang, C.H., Marr, M.T., and Rosbash, M. (2011). Nascent-seq indicates widespread cotranscriptional pre-mRNA splicing in Drosophila. Genes Dev *25*, 2502–2512. https://doi.org/10.1101/gad.178962.111.

Kierzek, E., Malgowska, M., Lisowiec, J., Turner, D.H., Gdaniec, Z., and Kierzek, R. (2014). The contribution of pseudouridine to stabilities and structure of RNAs. Nucleic Acids Res *42*, 3492–3501. https://doi.org/10.1093/nar/gkt1330.

Kim, D., Pertea, G., Trapnell, C., Pimentel, H., Kelley, R., and Salzberg, S.L. (2013). TopHat2: accurate alignment of transcriptomes in the presence of insertions, deletions and gene fusions. Genome Biol *14*, R36. https://doi.org/10.1186/gb-2013-14-4-r36.

Kim, M.H., You, B.H., and Nam, J.W. (2015). Global estimation of the 3′ untranslated region landscape using RNA sequencing. Methods *83*, 111–117. https://doi.org/10.1016/j.ymeth.2015.04.011.

Knight, S.W., Heiss, N.S., Vulliamy, T.J., Greschner, S., Stavrides, G., Pai, G.S., Lestringant, G., Varma, N., Mason, P.J., Dokal, I., and Poustka, A. (1999). X-linked dyskeratosis congenita is predominantly caused by missense mutations in the DKC1 gene. Am. J. Hum. Genet. *65*, 50–58. https://doi.org/10.1086/302446.

Koš, M., and Tollervey, D. (2010). Yeast pre-rRNA processing and modification occur cotranscriptionally. Mol. Cell *37*, 809–820. https://doi.org/10.1016/j.molcel.2010.02.024.

Langmead, B., and Salzberg, S.L. (2012). Fast gapped-read alignment with Bowtie 2. Nature Methods *9*, 357–359.

Lestrade, L., and Weber, M.J. (2006). snoRNA-LBME-db, a comprehensive database of human H/ACA and C/D box snoRNAs. Nucleic Acids Res *34*, D158–D162. https://doi.org/10.1093/nar/gkj002.

Li, X., Zhu, P., Ma, S., Song, J., Bai, J., Sun, F., and Yi, C. (2015). Chemical pulldown reveals dynamic pseudouridylation of the mammalian transcriptome. Nat. Chem. Biol. *11*, 592–597. https://doi.org/10.1038/nchembio.1836.

Liu, N., Dai, Q., Zheng, G., He, C., Parisien, M., and Pan, T. (2015). N6-methyladenosine-dependent RNA structural switches regulate RNA-protein interactions. Nature *518*, 560–564. https://doi.org/10.1038/nature14234.

Liu, N., and Pan, T. (2016). Probing N6-methyladenosine (m6A) RNA modification in total RNA with SCARLET. Methods Mol. Biol. *1358*, 285–292. https://doi.org/10.1007/978-1-4939-3067-8_17.

Love, M.I., Huber, W., and Anders, S. (2014). Moderated estimation of fold change and dispersion for RNA-seq data with DESeq2. Genome Biol *15*, 550. https://doi.org/10.1186/s13059-014-0550-8.

Lovejoy, A.F., Riordan, D.P., and Brown, P.O. (2014). Transcriptome-wide mapping of pseudouridines: pseudouridine synthases modify specific mRNAs in *S. cerevisiae*. PLoS One *9*, e110799. https://doi.org/10.1371/journal.pone.0110799.

Lynch, K.W., and Weiss, A. (2000). A model system for activation-induced alternative splicing of CD45 pre-mRNA in T cells implicates protein kinase C and Ras. Mol. Cell. Biol. *20*, 70–80. https://doi.org/10.1128/MCB.20.1.70-80.2000.

Mannoor, K., Liao, J., and Jiang, F. (2012). Small nucleolar RNAs in cancer. Biochim. Biophys. Acta *1826*, 121–128. https://doi.org/10.1016/j.bbcan.2012.03.005.

Marceau, C.D., Puschnik, A.S., Majzoub, K., Ooi, Y.S., Brewer, S.M., Fuchs, G., Swaminathan, K., Mata, M.A., Elias, J.E., Sarnow, P., and Carette, J.E. (2016). Genetic dissection of Flaviviridae host factors through genome-scale CRISPR screens. Nature *535*, 159–163. https://doi.org/10.1038/nature18631.

Martin, M. (2011). Cutadapt removes adapter sequences from high-throughput sequencing reads. EMBnet J. *17*, 10. https://doi.org/10.14806/ej.17.1.200.

Martinez, N.M., and Gilbert, W.V. (2018). Pre-mRNA modifications and their role in nuclear processing. Quant. Biol. *6*, 210–227. https://doi.org/10.1007/s40484-018-0147-4.

Martinez, N.M., and Gilbert, W.V. (2021). Investigating pseudouridylation mechanisms by high-throughput *in vitro* RNA pseudouridylation and sequencing. Methods Mol. Biol. *2298*, 379–397.

Martinez, N.M., Schaening-Burgos, C., and Gilbert, W.V. (2021). Pseudouridine site assignment by high-throughput *in vitro* RNA pseudouridylation and sequencing. Methods Enzymol *658*, 277–310. https://doi.org/10.1016/bs.mie.2021.06.026.

Massenet, S., Motorin, Y., Lafontaine, D.L., Hurt, E.C., Grosjean, H., and Branlant, C. (1999). Pseudouridine mapping in the *Saccharomyces cerevisiae* spliceosomal U small nuclear RNAs (snRNAs) reveals that pseudouridine synthase Pus1p exhibits a dual substrate specificity for U2 snRNA and tRNA. Mol. Cell. Biol. *19*, 2142–2154.

McGovern, D.P.B., Gardet, A., Törkvist, L., Goyette, P., Essers, J., Taylor, K.D., Neale, B.M., Ong, R.T., Lagacé, C., Li, C., et al. (2010). Genome-wide association identifies multiple ulcerative colitis susceptibility loci. Nat. Genet. *42*, 332–337. https://doi.org/10.1038/ng.549.

McMahon, M., Contreras, A., and Ruggero, D. (2015). Small RNAs with big implications: new insights into H/ACA snoRNA function and their role in human disease. Wiley Interdiscip. Rev. RNA *6*, 173–189. https://doi.org/10.1002/wrna.1266.

Mercer, T.R., Clark, M.B., Andersen, S.B., Brunck, M.E., Haerty, W., Crawford, J., Taft, R.J., Nielsen, L.K., Dinger, M.E., and Mattick, J.S. (2015). Genome-wide discovery of human splicing branchpoints. Genome Res *25*, 290–303. https://doi.org/10.1101/gr.182899.114.

Mi, H., Muruganujan, A., and Thomas, P.D. (2013). PANTHER in 2013: modeling the evolution of gene function, and other gene attributes, in the context of phylogenetic trees. Nucleic Acids Res *41*, D377–D386. https://doi.org/10.1093/nar/gks1118.

Newby, M.I., and Greenbaum, N.L. (2001). A conserved pseudouridine modification in eukaryotic U2 snRNA induces a change in branch-site architecture. RNA *7*, 833–845. https://doi.org/10.1017/S1355838201002308.

Nussbacher, J.K., and Yeo, G.W. (2018). Systematic discovery of RNA binding proteins that regulate microRNA levels. Mol. Cell *69*, 1005–1016.e7. https://doi.org/10.1016/j.molcel.2018.02.012.

Pan, H., Luo, C., Li, R., Qiao, A., Zhang, L., Mines, M., Nyanda, A.M., Zhang, J., and Fan, G.-H. (2008). Cyclophilin A is required for CXCR4-mediated nuclear export of heterogeneous nuclear ribonucleoprotein A2, activation and nuclear translocation of ERK1/2, and chemotactic cell migration. J. Biol. Chem. *283*, 623–637. https://doi.org/10.1074/jbc.M704934200.

Pandya-Jones, A., Bhatt, D.M., Lin, C.-H., Tong, A.-J., Smale, S.T., and Black, D.L. (2013). Splicing kinetics and transcript release from the chromatin compartment limit the rate of lipid A-induced gene expression. RNA *19*, 811–827. https://doi.org/10.1261/rna.039081.113.

Pineda, J.M.B., and Bradley, R.K. (2018). Most human introns are recognized via multiple and tissue-specific branchpoints. Genes Dev. *32*, 577–591. https://doi.org/10.1101/gad.312058.118.

Quinlan, A.R., and Hall, I.M. (2010). BEDTools: a flexible suite of utilities for comparing genomic features. Bioinformatics *26*, 841–842. https://doi.org/10.1093/bioinformatics/btq033.

Repnik, K., and Potočnik, U. (2016). eQTL analysis links inflammatory bowel disease associated 1q21 locus to ECM1 gene. J. Appl. Genet. *57*, 363–372. https://doi.org/10.1007/s13353-015-0334-1.

Roundtree, I.A., Evans, M.E., Pan, T., and He, C. (2017). Dynamic RNA modifications in gene expression regulation. Cell *169*, 1187–1200. https://doi.org/10.1016/j.cell.2017.05.045.

Safra, M., Nir, R., Farouq, D., Vainberg Slutskin, I., and Schwartz, S. (2017). TRUB1 is the predominant pseudouridine synthase acting on mammalian mRNA via a predictable and conserved code. Genome Res *27*, 393–406. https://doi.org/10.1101/gr.207613.116.

Schattner, P., Brooks, A.N., and Lowe, T.M. (2005). The tRNAscan-SE, snoscan and snoGPS web servers for the detection of tRNAs and snoRNAs. Nucleic Acids Res *33*, W686–W689. https://doi.org/10.1093/nar/gki366.

Schwartz, S., Bernstein, D.A., Mumbach, M.R., Jovanovic, M., Herbst, R.H., León-Ricardo, B.X., Engreitz, J.M., Guttman, M., Satija, R., Lander, E.S., et al. (2014). Transcriptome-wide mapping reveals widespread dynamic-regulated pseudouridylation of ncRNA and mRNA. Cell *159*, 148–162. https://doi.org/10.1016/j.cell.2014.08.028.

Shaheen, R., Han, L., Faqeih, E., Ewida, N., Alobeid, E., Phizicky, E.M., and Alkuraya, F.S. (2016). A homozygous truncating mutation in PUS3 expands the role of tRNA modification in normal cognition. Hum. Genet. *135*, 707–713. https://doi.org/10.1007/s00439-016-1665-7.

Shalem, O., Sanjana, N.E., Hartenian, E., Shi, X., Scott, D.A., Mikkelson, T., Heckl, D., Ebert, B.L., Root, D.E., Doench, J.G., and Zhang, F. (2014).

Genome-scale CRISPR-Cas9 knockout screening in human cells. Science *343*, 84–87. https://doi.org/10.1126/science.1247005.

Shen, S., Park, J.W., Lu, Z.X., Lin, L., Henry, M.D., Wu, Y.N., Zhou, Q., and Xing, Y. (2014). rMATS: robust and flexible detection of differential alternative splicing from replicate RNA-Seq data. Proc. Natl. Acad. Sci. USA *111*, E5593–E5601. https://doi.org/10.1073/pnas.1419161111.

Stadler, C., Rexhepaj, E., Singan, V.R., Murphy, R.F., Pepperkok, R., Uhlén, M., Simpson, J.C., and Lundberg, E. (2013). Immunofluorescence and fluorescent-protein tagging show high correlation for protein localization in mammalian cells. Nat. Methods *10*, 315–323. https://doi.org/10.1038/nmeth.2377.

Taggart, A.J., Lin, C.L., Shrestha, B., Heintzelman, C., Kim, S., and Fairbrother, W.G. (2017). Large-scale analysis of branchpoint usage across species and cell lines. Genome Res *27*, 639–649. https://doi.org/10.1101/gr.202820.115.

Taoka, M., Nobe, Y., Yamaki, Y., Sato, K., Ishikawa, H., Izumikawa, K., Yamauchi, Y., Hirota, K., Nakayama, H., Takahashi, N., et al. (2018). Landscape of the complete RNA chemical modifications in the human 80S ribosome. Nucleic Acids Res *46*, 9289–9298. https://doi.org/10.1093/nar/gky811.

Thorenoor, N., and Slaby, O. (2015). Small nucleolar RNAs functioning and potential roles in cancer. Tumour Biol *36*, 41–53. https://doi.org/10.1007/s13277-014-2818-8.

Vaidyanathan, P.P., AlSadhan, I., Merriman, D.K., Al-Hashimi, H.M., and Herschlag, D. (2017). Pseudouridine and N(6)-methyladenosine modifications weaken PUF protein/RNA interactions. RNA *23*, 611–618. https://doi.org/10.1261/rna.060053.116.

Van Nostrand, E.L., Pratt, G.A., Shishkin, A.A., Gelboin-Burkhart, C., Fang, M.Y., Sundararaman, B., Blue, S.M., Nguyen, T.B., Surka, C., Elkins, K., et al. (2016). Robust transcriptome-wide discovery of RNA-binding protein binding sites with enhanced CLIP (eCLIP). Nat. Methods *13*, 508–514. https://doi.org/10.1038/nmeth.3810.

Van Nostrand, E.L. (2018). A large-scale binding and functional map of human RNA binding proteins. bioRxiv, bioRxiv:10.1101/179648.

Wang, T., Wei, J.J., Sabatini, D.M., and Lander, E.S. (2014). Genetic screens in human cells using the CRISPR-Cas9 system. Science *343*, 80–84. https://doi.org/10.1126/science.1246981.

Williams, G.T., and Farzaneh, F. (2012). Are snoRNAs and SnoRNA host genes new players in cancer? Nat. Rev. Cancer *12*, 84–88. https://doi.org/10.1038/nrc3195.

Wu, G., Yu, A.T., Kantartzis, A., and Yu, Y.T. (2011). Functions and mechanisms of spliceosomal small nuclear RNA pseudouridylation. Wiley Interdiscip. Rev. RNA *2*, 571–581. https://doi.org/10.1002/wrna.77.

Xia, Z., Donehower, L.A., Cooper, T.A., Neilson, J.R., Wheeler, D.A., Wagner, E.J., and Li, W. (2014). Dynamic analyses of alternative polyadenylation from RNA-seq reveal a 3′2-UTR landscape across seven tumour types. Nat. Commun. *5*, 5274. https://doi.org/10.1038/ncomms6274.

Zhao, Y., Karijolich, J., Glaunsinger, B., and Zhou, Q. (2016). Pseudouridylation of 7SK snRNA promotes 7SK snRNP formation to suppress HIV-1 transcription and escape from latency. EMBO Rep *17*, 1441–1451. https://doi.org/10.15252/embr.201642682.

Zong, F.-Y., Fu, X., Wei, W.-J., Luo, Y.-G., Heiner, M., Cao, L.-J., Fang, Z., Fang, R., Lu, D., Ji, H., and Hui, J. (2014). The RNA-binding protein QKI suppresses cancer-associated aberrant splicing. PLoS Genet *10*, e1004289. https://doi.org/10.1371/journal.pgen.1004289.

Please cite this article in press as: Martinez et al., Pseudouridine synthases modify human pre-mRNA co-transcriptionally and affect pre-mRNA processing, Molecular Cell (2021), https://doi.org/10.1016/j.molcel.2021.12.023

STAR★METHODS

KEY RESOURCES TABLE

REAGENT or RESOURCE	SOURCE	IDENTIFIER
Antibodies		
Rabbit polyclonal anti-PUS1	Bethyl Labs	Cat# A301-651A; RRID:AB_1211501
Mouse monoclonal anti-U1-70K	Millipore	Cat# 05-1588; RRID:AB_11210916
Rabbit polyclonal anti-GAPDH	Sigma-Aldrich	Cat# G9545; RRID:AB_796208
Rabbit polyclonal Anti-H3	Abcam	Cat# ab1791; RRID:AB_302613
Rabbit polyclonalanti-DKC1	GeneTex	Cat# GTX109000; RRID:AB_11165396
Goat anti-mouse IgG, HRP	Invitrogen	Cat# 62-6520; RRID:AB_2533947
Goat anti-rabbit IgG, HRP	Promega	Cat# W4011; RRID:AB_430833
Bacterial and virus strains		
One Shot™ Stbl3™ Chemically Competent *E. coli*	Invitrogen	C737303
NEB® Stable Competent *E. coli*	NEB	C3040H
BL21 (DE3) Gold cells	Agilent	230130
NEB® 5-alpha Competent *E. coli*	NEB	C2988J
Rosetta 2(DE3)pLysS Competent Cells	Novagen	71403-M
Chemicals, peptides, and recombinant proteins		
Polybrene	Millipore Sigma	TR-1003-G
TRIzol Reagent	Invitrogen	15596026
QIAzol Reagent	Qiagen	79306
X-tremeGene 9 Transfection Reagent	Millipore Sigma	6365787001
Lipofectamine 2000	Invitrogen	11668027
Benzonase Nuclease	Millipore Sigma	E1014-25KU
T4 PNK	NEB	M0201L
T4 DNA Ligase	NEB	M0202L
AMV RT	Promega	M5108
MMLV RT	NEB	M0253S
Taq Polymerase	NEB	M0273S
Phusion Polymerase	NEB	M0530L
Doxycycline hyclate	Sigma-Aldrich	D9891-1G
Puromycin dihydrochloride	Sigma-Aldrich	P7255-100MG
N-cyclohexyl-N′-(2-morpholinoethyl)carbodiimide metho-p- toluenesulfonate (CMC)	Sigma-Aldrich	C106402
BbsI	NEB	R0539S
NdeI	NEB	R0111S
XbaI	NEB	R0145S
hTRUB1	This paper	N/A
hPUS7	This paper	N/A
hPUS7L	This paper	N/A
TRUB2	This paper	N/A
RPUSD2	This paper	N/A
hPUS10	This paper	N/A
hPUS1	This paper	N/A
cOmplete™, Mini, EDTA-free Protease Inhibitor Cocktail	Roche	4693159001
Hyclone Fetal Bovine Serum	GE Healthcare	SH30071.03

(*Continued on next page*)

Please cite this article in press as: Martinez et al., Pseudouridine synthases modify human pre-mRNA co-transcriptionally and affect pre-mRNA processing, Molecular Cell (2021), https://doi.org/10.1016/j.molcel.2021.12.023

Continued

REAGENT or RESOURCE	SOURCE	IDENTIFIER
HyClone Dulbecco's Modified Eagle Medium (DMEM)	GE Healthcare	SH3022.FS
Critical commercial assays		
T7 MegaShortScript kit	Thermo Fisher Scientific	AM1345
rRNA depletion	Illumina	MRZH11124
Deposited data		
Raw and analyzed data	This paper	GEO: GSE123613
Experimental models: Cell lines		
HepG2	ATCC	HB-8065
HEK293T	ATCC	CRL-1573
Oligonucleotides		
PUS1upF 5′- CACCGCGCAGGGTCCACCGTCCGA -3′	This paper (IDT)	N/A
PUS1upR 5′- AAACTCGGACGGTGGACCCTGCGC -3′	This paper (IDT)	N/A
PUS1dnF 5′- CACCGATAACAGCGGTTAGCGGCA -3′	This paper (IDT)	N/A
PUS1dnR 5′- AAACTGCCGCTAACCGCTGTTATC -3′	This paper (IDT)	N/A
shPUS7_4F 5′- CCGGTCTTAGTTCAGACTCA TATATCTCGAGATATATGAGTCTGAACTAAG ATTTTTG -3′	This paper (IDT)	N/A
shPUS7_4R 5′- AATTCAAAAATCTTAGTTCAGA CTCATATATCTCGAGATATATGAGTCTGAAC TAAGA-3′	This paper (IDT)	N/A
shRPUSD4_2F 5′- CCGGGCTTCGAGTTCA CTTGTCCTTCTCGAGAAGGACAAGTGAAC TCGAAGCTTTTTG -3′	This paper (IDT)	N/A
shRPUSD4_2R 5′- AATTCAAAAAGCTTCG AGTTCACTTGTCCTTCTCGAGAAGGACA AGTGAACTCGAAGC -3′	This paper (IDT)	N/A
DNA pool of 6000 oligos	Twist Biosciences	GSE123613
Pool PCR F primer (oBZ131) 5′- GCTAATACGACTCACTATAGGG -3′	IDT	N/A
Pool PCR R primer (oTC_pool2_rev) 5′- GCTAATACGACTCACTATAGGG -3′	IDT	N/A
Pool RT primer (ONM_RT-L2) 5′- /5Phos/ NNNNNNNNNGATCGTCGGACTGTA GAACTCTGAACGTGTAGATC/iSp18/CACTC A/iSp18/CCTTGGCACCCGAGAATTCCAGTC CTTGGTGCCCGAGTG -3′	IDT	N/A
RP1 primer—Library PCR F 5′- AATGATACGGCGACCACCGAGATCTACAC GTTCAGAGTTCTACAGTCCGA -3′	IDT	N/A
Barcoded reverse PCR primers (XXXXXX indicates unique barcodes)—Library PCR R 5′-CAAGCAGAAGACGGCATACGAGATX XXXXXGTGACTGGAGTTCCTTGGCACCC GAGAATTCCA -3′	IDT	N/A
In cell Pseudo-seq RT primer 5′-/5Phos/ GATCGTCGGACTGTAGAACTCTGAACC TGTCGGTGGTCGCCGTATCATT/ iSp18 /CACTCA/iSp18/GCCTTGGC ACCCGAGAATTCCA -3′	IDT	N/A

(*Continued on next page*)

Continued

REAGENT or RESOURCE	SOURCE	IDENTIFIER
In cell Pseudo-seq–Library PCR F 5′- AATGATACGGCGACCACCGA -3′	IDT	N/A
RBM39 splicing reporter GBlock TAGAAACTG GGCATATGATTTGAATGAACCCTGCTATTG TAGTCCTCTTTTATTAATG CTTTCCTGACAT TTACCCTGTTAGTTGAGGCTCTTCATTGTT CCTGCACTGAGCTGTA GAATTCTCTTTT GTTATAGATTTGCAAACAAGACTTTCCCA GCAGACTGAAGTCTAG AGGGCCCGTTT	This paper (IDT)	N/A
RBM39 splicing reporter GBlock TAGAAACTGGGCATATGGCTTTAGTTTTAAC TGTTGTTTATGTTCTTTATATATGATG TATTTTCCACAGATGTTTCATGATTTCCAGTT TTCATCGTGTCttttttttCCTTGTAGGCAA AT GTGCAATACCAACATGTCTGTACCTACT GATGGTGCTGTAACCACCTCACAGATT CCAGCTTCGGAACAAGAGACCCTGTCT AGAGGGCCCGTTT.	This paper (IDT)	N/A
GE1-F 5′- GCAAGGTGAACGTGGATGAAGTTGG – 3′	IDT	N/A
MDM2_E-R 5′- CAGGGTCTCTTGTTCCGAAGCTGG -3′	IDT	N/A
RBM39_E-R 5′- CAGTCTGCTGGGAAAGTCTTGTTTGC -3′	IDT	N/A
U2snRNA_ext_sh 5′- CCTCGGATAGAGGACGTATCAG -3′	IDT	N/A
U2snRNA_ext_lo 5′- TACCAGGTCGATGCGTGG -3′	IDT	N/A
Recombinant DNA		
pSpCas9(BB)-2A-GFP (PX458)	Addgene	48138
Tet-pLKO-puro	Addgene	21915
pCMV-dR8.2	Addgene	8455
pCMV-VSV-G	Addgene	8454
pcAT7-Glo1	Gift from Kristen Lynch	N/A
Software and algorithms		
Bowtie 2	(Langmead and Salzberg, 2012)	http://bowtie-bio.sourceforge.net/bowtie2/index.shtml
Tophat2	Kim et al., 2013	https://ccb.jhu.edu/software/tophat/index.shtml
STAR	Dobin et al., 2013	https://github.com/alexdobin/STAR
Cutadapt	Martin, 2011	https://cutadapt.readthedocs.io/en/stable/
rMATS	(Shen et al., 2014)	http://rnaseq-mats.sourceforge.net
MEME Suite	Bailey et al., 2015	https://meme-suite.org/meme/
HTseq	(Anders et al., 2015)	https://htseq.readthedocs.io/en/master/
DEseq2	Love et al., 2014	http://www.bioconductor.org/packages/release/bioc/html/DESeq2.html
QAPA	Ha et al., 2018	https://github.com/morrislab/qapa
Bedtools	(Quinlan and Hall, 2010)	https://bedtools.readthedocs.io/en/latest/

RESOURCE AVAILABILITY

Lead contact

Further information and requests for reagents may be directed to and will be fulfilled by the lead contact, Wendy V. Gilbert (wendy.gilbert@yale.edu).

Materials availability

This study did not generate new unique reagents.

Data and code availability

- All sequencing and annotations data have been deposited at GEO and are publicly available as of the date of publication.
- This paper does not report original code.
- Any additional information required to reanalyze the data reported in this paper is available from the lead contact upon request.

EXPERIMENTAL MODEL AND SUBJECT DETAILS

Cell culture

Human hepatocellular carcinoma cells HepG2 from ATCC HB8065 (lot 59635738) were grown in DMEM (HyClone SH30022.FS) supplemented with 10% fetal bovine serum (FBS HyClone SH30071.03). Cells were grown at 37C with 5% CO2 and maintained at subconfluency.

METHOD DETAILS

Total RNA Isolation

HepG2 cells were harvested by pelleting and resuspending fresh or frozen (-80C) pellets in 1mL of QIAzol (Qiagen). Total RNA was harvested according to the manufacturer's procedure.

Western Blotting

Whole cell lysates were made by pelleting HepG2 cells and re-suspending fresh or frozen (-80C) pellets in RIPA buffer (50mM Tris pH 8, 150 mM NaCl, sodium deoxycholate 0.5%, sodium dodecyl sulfate 0.1%, NP-40 1%), lysed on ice for 10 min with vortexing. Spun down at 4C and maximum speed (13,200 rpm) for 15 min and collected supernatant as lysate. Approximately, 20ug of whole cell lysates, as determined by Bradford assay, were loaded in 10% SDS-PAGE for western blot of PUS1 knockout and wildtype HepG2 cells. HepG2 fractions were isolated as described below and treated with Benzonuclease to release proteins from nucleic acid. Equal cell volumes of cellular fractions (3%) were loaded in 12% SDS-PAGE gels for Western blots of cell compartments to determine fraction purity. Gels were transferred to nitrocellulose membranes. Membranes were blocked in 5% milk and incubated with primary antibodies overnight at 4C in 5% milk low-salt TBST (50 mM Tris pH 7.5 150 mM NaCl 0.1% Tween-20). Antibodies used for Western blot were as follows: anti-PUS1 at 1:1000 (Bethyl Labs A301-651A), anti-U1-70K at 1:2000 (Millipore 05-1588), anti-GAPDH at 1:10,000 (Sigma-Aldrich G9545), anti-H3 at 1:20,000 and anti-DKC1 at 1:1000 (GeneTex GTX109000). Secondary antibody incubation was for 1 hour at room temperature using HRP conjugated antibodies: anti-mouse IgG at 1:3000(Invitrogen 62–6520) or goat anti-rabbit IgG at 1:3000 (Promega W4011). Washes were with high-salt TBST (50 mM Tris pH 7.5 400 mM NaCl 0.1% Tween-20).

CRISPR knockout generation

PUS1 CRISPR knockout HepG2 cells were generated using a two-guide strategy to take out the first exon containing the translation start codon. Oligos for the upstream PUS1upF 5′- CACCGCGCAGGGTCCACCGTCCGA -3′ and PUS1upR 5′- AAACTCGGACGGTGGACCCTGCGC -3′, and for the downstream guide PUS1dnF 5′- CACCGATAACAGCGGTTAGCGGCA -3′ and PUS1dnR 5′- AAACTGCCGCTAACCGCTGTTATC -3′ were phosphorylated and annealed and then cloned into px458 (Addgene) digested with BbsI. HepG2 cells were transfected with both plasmids for the upstream guide and downstream guide (1.25 μg of each) with Lipofectamine 2000 according to the manufacturer's protocol in 6-well plates. After 24h the cells were visually inspected for GFP fluorescence and prepared for sorting by trypsinizing and re-suspended in FACS buffer (PBS without Mg2+ and Ca2+ and supplemented with 2% FBS). Single GFP positive cells were sorted on an Aria I sorter and plated into each well of a 96 well plate. PUS1 knockout clones were expanded and knockout verified by PCR of genomic DNA and Western Blot with anti-PUS1.

PUS protein depletion

shRNAs targeting PUS7 and RPUSD4 were cloned into the lentiviral vector pLKO-Tet-On (Addgene) digested with AgeI-HF and EcoRI-HF to remove the stuffer sequence. Two oligos containing the complementary shRNA targeting sequence with the corresponding overhangs were annealed and ligated into the vector by standard cloning. Oligos sequences for RPUSD4 and PUS7 were:

Please cite this article in press as: Martinez et al., Pseudouridine synthases modify human pre-mRNA co-transcriptionally and affect pre-mRNA processing, Molecular Cell (2021), https://doi.org/10.1016/j.molcel.2021.12.023

shRPUSD4_2F

5′- CCGGGCTTCGAGTTCACTTGTCCTTCTCGAGAAGGACAAGTGAACTCGAAGCTTTTTG-3′, shRPUSD4_2R, 5′- AATTCAAAAAGCTTCGAGTTCACTTGTCCTTCTCGAGAAGGACAAGTGAACTCGAAGC-3′

shPUS7_4F

5′- CCGGTCTTAGTTCAGACTCATATATCTCGAGATATATGAGTCTGAACTAAGATTTTTG-3′

shPUS7_4R

5′- AATTCAAAAATCTTAGTTCAGACTCATATATCTCGAGATATATGAGTCTGAACTAAGA-3′.

Lentiviral particles were prepared by transfecting a 10cm dish of HEK293T cells with 5μg pLKO-Tet-On, 4.5μg pCMV-dR8.2, 500ng pCMV-VSV-G and transfection reagent X-tremeGENE 9 according to the manufacturer's protopcol. Viral supernatant was harvested 48h after transfection. HepG2 cells were transduced in 6-well plate with 1mL of viral supernatant in 6 well plates with 1mL of cell suspension. Cells stably integrated with the lentiviral vector were selected 48h post-transduction with 3μg/mL of puromycin until cells in the untransduced cells did not survive. shRNA expression was induced in HepG2 cells with Doxocycline to a final concentration of 500 ng/mL. Cells were maintained in Doxoxycline containing media for 96h and whole cell lysates were prepared for Western Blot analysis of depletion and RNA was isolated for RNA-seq library construction.

Nuclear extract preparation

HepG2 cells were pelleted by spinning down at 1000 rpm for 5 min, washed with PBS. Cells were transferred to 1.5 mL tube and centrifuged at 3000 rpm for 1 minute. The pellet was re-suspended in cytoplasmic extract buffer (10 mM HEPES pH 7.6, 1.5 mM $MgCl_2$, 10 mM KCl, 0.15% NP-40) ~100 μL per 2x10^6 cells and incubated on ice for 5 minutes and spun down for 3 min at 6500 rpm for 3 minutes. Supernatant was collected as cytoplasmic fraction. The nuclear pellet was re-suspended in equal volume of nuclear extract buffer (20 mM HEPES pH 7.6, 1.5 mM $MgCl_2$, 420 mM NaCl, 0.2 mM EDTA, 20% glycerol). Three cycles of 15 minutes at -80C followed by thawing at 37C with vortexing for 1 minute in between cycles. Spun down at max speed for 15 minutes at 4C. Collected supernatant as nuclear extract.

Cellular Fractionation

Biochemical fractionation was performed essentially as described in (Bhatt et al., 2012; Pandya-Jones et al., 2013) for 11 biological replicates of HepG2 cells. All fractions were prepared from fresh cell pellets. Two 10 cm dishes with ~10x10^6 each of HepG2 cells were trypsinized and spun down at 500xg and washed with cold PBS (1mM EDTA). Cell pellets were re-suspended in 400 μL of cytoplasmic NP-40 lysis buffer (10 mM Tris-HCl pH 7.5, 0.15% NP-40, 150 mM NaCl) by flicking tube and incubated on ice for 5 minutes. Lysate was layered over 1 mL of sucrose cushion (24% RNAse-free sucrose in cytoplasmic lysis buffer) and spun down 10 minutes at 15,000xg at 4°C. Supernatant was collected as cytoplasmic fraction. Nuclear pellet was washed 2x with PBS without displacing pellet (1mM EDTA) and re-suspended in 200 μL glycerol buffer (20 mM Tris-HCl pH 7.9, 75 mM NaCl, 0.5 mM EDTA, 0.85 mM DTT, 0.125 mM PMSF, 50% glycerol) by flicking tube followed by addition of 200 μL of nuclei lysis buffer (10 mM HEPES pH 7.6, 1 mM DTT, 7.5 mM $MgCl_2$, 0.2 mM EDTA, 0.3 M NaCl, 1 M UREA, 1% NP-40). Samples were then vortexed on high 2x 2 seconds, incubated on ice for 2 minutes, centrifuged for 2 min at 4°C 15,000xg and the supernatant collected as nucleoplasmic fraction. The remaining chromatin pellet was washed 2x with PBS without displacing pellet (1mM EDTA) and re-suspended in 100uL of PBS (1mM EDTA). DNase I (2uL NEB) was added to re-suspended chromatin-pellet and incubated at 37°C for 5-10 minutes to dissolve pellet. Collected 10uL for western blot of fractions and added 1mL of QIAzol (Qiagen) to remaining chromatin and incubated at 50°C for 10 min to solubilize chromatin. Followed manufacturer's instruction to finish isolating chromatin-associated RNA with QIAzol. Samples were DNase I treated (NEB) treated after QIAzol isolation according to manufacturer's instructions.

rRNA depletion

Ribosomal RNA (rRNA) was depleted using one Ribozero (Illumina MRZH11124) reaction per 20ug of chromatin-associated RNA following the manufacturer's protocol.

Recombinant PUS plasmids and purification

Human TRUB1, PUS7, PUS7L, TRUB2, RPUSD2 and PUS10 were cloned from human cDNA obtained from Human ORFeome (cDNA from Mammalian Gene Collection) with Gibson assembly into the BamH1 site of pET15b expression. Recombinant hPus1 was purified as described (Czudnochowski et al., 2013). Expression was induced in BL21 (DE3) Gold cells [Agilent] with 0.1 mM IPTG at OD600 0.6-0.8. Cells were grown overnight at 16°C, then harvested by centrifugation and resuspended in lysis buffer (50 mM HEPES-KOH pH 7.0, 500 mM NaCl, 5 mM β-mercaptoethanol, 1x Protease Inhibitor Cocktail (Roche)) and lysed by sonication. Human PUS1 was induced and the bacterial lysate was centrifuged at 12,000 rpm for 30 min, bound on a HisTrap column (GE Healthcare) and eluted off the column with 250 mM imidazole. The protein was then dialyzed overnight at 4°C into storage buffer (50 mM HEPES-KOH pH 7.0, 100 mM NaCl, 1 mM β-mercaptoethanol) and further purified by gel filtration over a Superdex-200 column (GE Healthcare). The protein product was concentrated with a centrifugal filter unit (MD Millipore) and concentration determined by Bradford staining against a BSA standard. Human TRUB1, PUS7, PUS7L, TRUB2, RPUSD2 and PUS10 were purified as follows. Rosetta 2 BL21 (DE3) pLysS cells were transformed with the expression vector and an individual colony was grown at 37°C in LB to OD600 0.8. Induction of expression was overnight at 18°C with 1mM IPTG. Protein was affinity purified using the HisTrap HP 5mL column

(GE) on an FPLC. Bound protein was washed with wash buffer (50mM potassium phosphate buffer pH 8, 0.5M NaCl, 30mM Imidazole) and then eluted with elution buffer (50mM potassium phosphate buffer pH 8, 0.5M NaCl, 300mM Imidazole). Protein was concentrated with Amicon Ultra Centrifugal Filter Units and stored in storage buffer containing 20mM HEPES (pH 7.5), 200mM NaCl, 10% glycerol, and 1mM DTT. Concentration was determined by Bradford with BSA standards.

In vitro pseudouridylation

A pool of 6000 DNA oligos (Twist Biosciences) was designed to contain all the sites identified as pseudouridines in chromatin-associated RNA from HepG2 cells. The DNA oligos in the pool contained 65 nucleotides upstream and 64 nucleotides downstream of the pseudouridine. In addition, the sequences contained the T7 promoter and a 3′ adapter sequence to serve as handles for PCR amplification. The pool was amplified by PCR with primers oBZ131 (GCTAATACGACTCACTATAGGG) and oTC_pool2_rev (GTCCTTGGTGCCCGAGTG) using Phusion Polymerase (NEB). PCR reactions were supplemented with 3% DMSO and gel purified prior to in vitro transcription. RNA was in vitro transcribed with the MEGAshortscript T7 transcription kit (Thermo Fisher) and gel purified. RNA was re-suspended in water, denatured at 75C for 2 min, cooled on ice for 5 min and folded at 37C for 20 min following addition of 5X pseudouridylation buffer (500 mM Tris pH 8.0, 500 mM Ammonium Acetate, 25 mM MgCl2, 0.5 mM EDTA) to 1X for the final reaction volume. In vitro pseudouridylation reactions were carried out by incubating 15-30 pmol of folded RNA with 600nM recombinant human pseudouridine synthases: PUS1, PUS7, PUS7L PUS10, RPUSD2, RPUSD4, TRUB1, TRUB2, HepG2 nuclear extract or no PUS for 45 minutes at 30C in 500uL final reaction volumes extract in (1X pseudouridylation buffer, 2mM DTT). RNA was purified immediately by phenol chloroform extractions and isopropanol precipitated.

Pseudo-seq

Pseudo-seq libraries were prepared as previously described in detail (Carlile et al., 2015). Briefly, rRNA-depleted chromatin-associated RNA was fragmented in 10mM ZnOAc for 2 minutes at 60C. Fragmentation was quenched by addition of EDTA to 20mM. RNA was then either treated with CMC (0.4M final) or mock treated (-CMC) in BEU buffer for 45 min at 40C and CMC was reversed from Us and Gs by incubation in Sodium carbonate buffer for 2 hours at 50C. RNA fragments 120-140 nucleotides in length were size selected from denaturing polyacrylamide gels for library preparation. The ends of the fragmented RNA were repaired by treatment with T4 Polynucleotide Kinase (NEB) and Calf intestinal alkaline phosphatase (NEB) in 1X PNK buffer (NEB). A 3′ adenylated adapter (AppTGGAATTCTCGGGTGCCAAGG/3ddC/) was ligated to the RNA fragments with T4 RNA ligase in 1X T4 RNA ligase buffer (NEB), followed by reverse transcription with AMV RT (Promega) and RT primer: /5Phos/GATCGTCGGACTGTAGAACTCTGAACCTGTCGGTGGTCGCCGTATCATT/iSp18/CACTCA/iSp18/GCCTTGGCACCCGAGAATTCCA. Truncated cDNAs (120-170nt) were size selected from denaturing polyacrylamide gels and gel purified cDNAs were circularized with CircLigase ssDNA ligase (Epicentre). Circularized cDNAs were PCR amplified with forward primer (AATGATACGGCGACCACCGA) and BC reverse primer (CAAGCAGAAGACGGCATACGAGATXXXXXXGTGACTGGAGTTCCTTGGCACCCGAGAATTCCA where Xs represent the unique barcode sequence). In vitro Pseudo-seq libraries were prepared as described above (Martinez and Gilbert, 2021) except with full length in vitro transcribed RNA recovered from in vitro pseudouridylation assays. After CMC modification and reversal, full length RNA was gel purified in denaturing polyacrylamide gels. Reverse transcription was performed using the 3′ adapter sequence appended to the pool oligos as a handle with RT primer ONM_RT-L2 (/5Phos/NNNNNNNNNGATCGTCGGACTGTAGAA CTCTGAACGTGTAGATC/iSp18/CACTCA/iSp18/CCTTGGCACCCGAGAATTCCAGTCCTTGGTGCCCGAGTG), truncated cDNAs from 140-170 nts were size selected and circularized for PCR amplification with primers RP1 (AATGATACGGCGACCACCGAGATCTACACGTT CAGAGTTCTACAGTCCGA) and BC reverse primer. Libraries were sequenced on an Illumina HiSeq in single-end mode to 20-30 million reads per sample for in vivo Pseudo-seq and 15-20 million reads for in vitro Pseudo-seq libraries.

RNA-seq

Total RNA was isolated for two replicates of wildtype and PUS1 knockout HepG2 cell as described above and stranded poly(A)+ selected mRNA-seq libraries were performed by the MIT BioMicroCenter using the TruSeq Stranded mRNA Library Prep Kit from Illumina according to the manufacturers' protocol. Libraries were sequenced on an Illumina Next-seq with paired end 40-bp reads to a depth of ~150 million paired reads per replicate. mRNA purity was comparable across libraries with 1.4% (WT1), 1.7% (WT2), 1.3% (KO1) and 1.3% (KO2) rRNA contamination. PUS7 (n=3) and RPUSD4 (n=2) knockdown stranded poly(A)+ selected mRNA-seq libraries were prepared by Genewiz and sequenced on a HiSeq with paired end 150-bp reads.

Sequencing Analysis

All sequencing data has been deposited in accession GEO: GSE123613. mRNA-seq reads were mapped to the human genome using STAR (Dobin et al., 2013) aligner. Reads were mapped to genome assembly GRCh37 with ENSEMBL GRCh37.75 annotations. STAR alignment was carried out using the following parameters: –outFilterType BySJout –outFilterMultimapNmax 20 –alignSJoverhangMin 8 –alignSJDBoverhangMin 1 –outFilterMismatchNmax 999 –alignIntronMin 20 –alignIntronMax 1000000 –alignMatesGapMax 1000000 –alignEndsType EndToEnd. Pseudo-seq sequencing data was analyzed using in house Bash and Python scripts. Cutadapt (Martin, 2011) was used to trim the 3′ adapter sequence from the reads. In vitro Pseudo-seq sequencing reads were also PCR duplicate collapsed using fastx_collapser (http://hannonlab.cshl.edu/fastx_toolkit/). Processed reads were mapped to a bowtie index of ENSEMBL GRCh37.75, 45S rRNA and snRNAs for in vivo Pseudo-seq libraries and the pool of sequences for in vitro Pseudo-seq libraries using tophat2 (Kim et al., 2013). The mapped reads were processed with in house Python scripts. Pseudo-seq signal or peak height was calculated as follows for all possible used annotated in GRCh37.75 excluding repetitive elements. For each U position centered on a 51-nucleotide window, the fraction of reads whose 5′ends map to the position was divided by the reads mapping to the window was calculated. Pseudo-seq signal is the difference in the fraction of reads between the +CMC and -CMC multiplied by the window size. For each Ψ the Pseudo-seq signal corresponds to that of the expected RT stop 1 nt 3′ of the Ψ site. Sites were called as pseudouridines if an RT stop with a peak height >1, met a read cutoff (reads/nt in the window) of 0.1 and was present in 7 out of 11 replicate libraries of chromatin-associated RNA.

PUS protein assignment

Peak heights for in vitro pseudouridylated sites were determined using the pipeline described previously in detail (Martinez et al., 2021). Briefly, peak heights were calculated based on a Z-score of read 5′ ends accumulating at the modified site relative to the background of other positions in a selected window in CMC-treated libraries as shown below.

Z-score = $\frac{reads_i - \mu}{\sigma}$ Where:

$reads_i$ = 5′ends at position

μ = avg 5'ends at each position in window

σ = standard deviation of 5' ends counts in window

Size selection of cDNA can lead to coverage biases. A window from positions 60 to 95 was selected as the background for the Z-score calculation based on the distribution of reads covering the RNA oligos. Z-scores are calculated for each putative psi position in the RNA pool and sites are assigned as modified by a particular PUS by selecting cutoffs such that the modified sites have Z-scores greater than the background of all other sites within each library and compared to a library prepared without addition of a pseudouridine synthase (no PUS). We plotted the distribution of Z-scores for each library as an inverse CDF. We chose cutoffs corresponding to the inflection point where the modified sites diverged from background sites within the same library and from the CMC-treated no PUS) library (Figure S4B). We also required that the Z-score be higher than in a mock treated (-CMC) library to ensure the peak is CMC-dependent. For the libraries in (Figure S4B) the cutoffs were set as follows: PUS7_plusCMC > 5, noPUS_plusCMC < 4 and Zdiff (PUSplusCMC – minusCMC) >= 2. This approach allows us to assign sites as targets of more than one PUS in the case that more than one enzyme modifies the same site and allows us to compare data generated from different experiments.

Alternative splicing analysis

Analysis of differential alternative splicing between wildtype and PUS1 KO HepG2 mRNA-seq was carried out by rMATS (version 3.) using Ensembl GRCh37.72 annotations. rMATS reported differences in alternative splicing of types skipped exons (SE), alternative 3′ splice sites (A3SS), alternative 5′ splice sites (A5SS), retained introns (RI) and mutually exclusive exons. Percent inclusion differences were determined from the rMATS junction only output files. Events with an absolute difference in percent inclusion between PUS1 KO and WT cells of greater than or equal to 10% and with and false discovery rate (FDR) of equal to or less than 0.05 are considered significant and reported.

Differential gene expression analysis

HTseq (version 0.6.1) was used to generate read counts tables that were submitted to DESeq2 (Love et al., 2014)(version 1.14.1) to determine differences in mRNA abundance between PUS1 KO, RPUSD4 KD or PUS7 KD and WT HepG2 cells from mRNA-seq data. After DESeq analysis genes with 0 counts in at least one sample were filtered out. Differences in mRNA levels with Padj < 0.05 were considered significant.

Enrichment analysis

Bedtools was used for overlapping pseudouridines and uridines with genomic features. As a background set for calculating the enrichment of pseudouridines in different regions we used all the uridines that met our read cutoff of 0.1 in our replicate cutoff of 7 out of 11, as was used for pseudouridine calling. Detected pseudouridines were classified into features according to gencode v19 annotations according to the following priority snoRNAs > lincRNAs > snRNA > miRNAs > antisense ncRNAs > 5′ UTR > 3′ UTR > exons > introns. Retained introns were filtered as introns. Enrichments of pseudouridines in the introns of alternatively spliced regions was carried out by overlapping intronic pseudouridines compared to uridines with MISO version 2 annotations (https://miso.readthedocs.io/en/fastmiso/annotation.html) which were generated from Ensembl genes, known Genes (UCSC) and RefSeq genes annotations. We compared the distribution of pseudouridines to uridines that we detected in introns flanking alternatively spliced region categories obtained as described above (Figure 2B). A a chi-squared test for the overall difference in proportions across categories for pseudouridines compared to uridines was applied to evaluate the significance of the difference in the distribution.(p-value = $2.2e^{-16}$). We compared the observed pseudouridine distribution to the uridine distribution for uridines that were captured in our sequencing assay to correct for uridine content and coverage bias. The distribution for pseudouridines relative to splice sites was compared to the distribution of detected uridines in proximal introns (within 500nt of splice sites) and splice sites (within 6 nt from exon ends). A hypergeometric test was applied (Fisher's exact test) to determine the significant in the observed enrichment of pseudouridines in these regions. P-values < 0.05 were considered significant. Pseudouridines were considered as present in branch site regions if they overlapped annotated branch site regions (Mercer et al., 2015; Taggart et al., 2017; Pineda and Bradley, 2018).

Pseudouridines were classified as present in putative PPT tracts if they were within 50 nucleotides of the 3′ splice site AG and by manual inspection.

Motif enrichment

131 nucleotides of sequence surrounding pseudouridine was used as the input to MEME (Bailey et al., 2015) version 5.0.2 in discriminative mode to identify motifs enriched in pseudouridine compared to the 131 nucleotides of sequence flanking the background set of uridines that met our read cutoff for pseudouridine calling in the Pseudo-seq libraries. Significantly enriched motifs are presented.

GO analysis

Gene ontology analysis was performed for pseudouridine containing genes using PANTHER version 11 (Mi et al., 2013). All Ensembl gene IDs for pseudouridine containing genes were used as the test set and the Ensembl gene IDs for all genes that contained uridines matching our read cutoff for pseudouridine identification (Table S1D). Reported enriched GO terms correspond to those that were significant after Bonferroni correction for multiple hypothesis testing.

Analysis of RBP eCLIP overlap with pseudouridines

Size matched input-normalized bed files for eCLIP biological replicates were combined into a single bedtool of shared peaks using bedtools intersect, where a shared peak was defined as at least one intersecting nucleotide. eCLIP peaks at pseudouridines in HepG2 cells were then identified by using bedtools intersect to determine eCLIP peaks where the peak overlapped with a pseudouridine. Volcano plots of these pseudouridine intersecting eCLIP peaks were then generated using the eCLIP $\log_2$(fold change) and Padj (Van Nostrand et al., 2016) values. We selected significance cutoffs of $\log_2$(fold change) of 2 and $-\log_{10}$(Padj) of 3. For the volcano plots, if an RBP had multiple pseudouridines within an eCLIP peak, we plotted the best cluster as defined by first the lowest Padj and highest fold change values. Introns were determined by the genic location using gencode hg19 annotations. To identify pseudouridine-interacting RBPs we ranked RBPs for preferential binding to pseudouridine sites. We calculated the fraction of significant eCLIP peaks that intersected pseudouridine sites over the total number of significant eCLIP peaks, then compared this ratio to one calculated using pseudouridine sites shuffled within introns. We performed this calculation with 1000 iterations of shuffling the pseudouridine location in introns to calculate a standard distribution of this ratio, and then calculated the z-score of the observed ratio. To filter for RBPs that bind uridine-rich motifs, we performed the same calculation with all high-confidence uridines that did not have a pseudouridine and repeated the 1000 iterations of shuffling and measuring the intersection with the RBPs.

In vitro splicing from nuclear extracts

The splicing reporter backbone pcAT7-Glo1 was digested with NdeI and XbaI and Gblocks including the entire endogenous exon and 100nt of intronic sequence (including the pseudouridylated position) and 15nt of vector overlapping sequence. The Gblock sequences are:

RBM39 TAGAAACTGGGCATATGATTTGAATGAACCCTGCTATTGTAGTCCTCTTTTATTAATGCTTTCCTGACATTTACCCTGTTAGTTGAGGCTCTTCATTGTTCCTGCACTGAGCTGTAGAATTCTCTTTTGTTATAGATTTGCAAACAAGACTTTCCCAGCAGACTGAAGTCTAGAGGGCCCGTTT

MDM2

TAGAAACTGGGCATATGGCTTTAGTTTTAACTGTTGTTTATGTTCTTTATATATGATGTATTTTCCACAGATGTTTCATGATTTCCAGTTTTCATCGTGTCttttttttCCTTGTAGGCAAATGTGCAATACCAACATGTCTGTACCTACTGATGGTGCTGTAACCACCTCACAGATTCCAGCTTCGGAACAAGAGACCCTGTCTAGAGGGCCCGTTT.

Plasmids were *in vitro* transcribed and subsequently linearized by restriction digest with XbaI.

Splicing reporter RNA (30pmol) were mock treated for unmodified or *in vitro* pseudouridylated with recombinant human PUS7 as described in the *in vitro* pseudouridylation section. Purified RNA substrates (15 pmol) were incubated with 32% Jurkat or HeLa nuclear extract in a total volume of 13 uL under splicing conditions 11.5 mM Tris-HCl, pH7.5, 3.0 mM MgCl2, 1 mM ATP, 20 mM CP, 0.5 mM DTT, 58 mM KCl, 3% PVA, 0.1 mM EDTA, and 11.5% glycerol.

Reactions were incubated for 30-60 min at 30°C or indicated time points. RNA was recovered from the reactions by proteinase K treatment, phenol- chloroform extraction and ethanol precipitation. The RNAs from the splicing reactions were analyzed by RT-PCR performed and analyzed as previously described in using reporter and gene-specific primers and a low cycle number (Lynch and Weiss, 2000). Primer sequences for reporter specific primers GE1-F – 5′- GCAAGGTGAACGTGGATGAAGTTGG – 3′ and for gene-specific primers MDM2_E-R 5′- CAGGGTCTCTTGTTCCGAAGCTGG -3′ or RBM39_E-R 5′- CAGTCTGCTGGGAAAGTCTTGTTTGC -3′.

Site lists and reproducibility analyses

We obtained lists of pseudouridine sites called in two publications: the initial list from our group, published in Table S8 of Carlile et al. (2014), and those reported in Table S1G of Khoddami et al. (2019). For Extended Data Figure 1B, we compared the lists reported by either publication and categorized them into sets, based on whether they had been called by either or both of these methods. For Extended Data Figure 1C, we additionally determined the sites that had been called in any of the following publications: (a) Schwartz

Please cite this article in press as: Martinez et al., Pseudouridine synthases modify human pre-mRNA co-transcriptionally and affect pre-mRNA processing, Molecular Cell (2021), https://doi.org/10.1016/j.molcel.2021.12.023

et al. (2014), which called sites transcriptome wide in HEK293 cells, rather than HeLa; (b) Carlile et al. (2019), which used an in vitro approach to validate sites (c) Li et al. (2015). We then used the UpSetR package (version 1.4.0) to visualize the reproducibility of the Carlile et al. (2014) sites across these datasets. ROC curves for HepG2 CARNA were generated based on a list of true positive sites corresponding know pseudouridine positions in the mature human 28S, 18S and 5.8S rRNA (Lestrade and Weber, 2006; Taoka et al., 2018) as previously described (Carlile et al., 2014). Pseudo-seq signal was calculated 1 nt 3′ to each known pseudouridine. A range of 500 equally spaced cutoff scores were chosen spanning the range of observed peak values. At each cutoff score, the true positive and false positive rates were calculated, and plotted. False positive rate was calculated for chosen cutoffs used for site calling in HepG2 chromatin-associated RNA (see Figure S1A; Table S1).

Sequence context analyses

For each set of sites in Extended Data Figure 1B, we generated a fasta file that contained the 11-nt sequence surrounding the pseudouridine site. We then used Weblogo 3 to visualize the frequency of each nucleotide relative to the pseudouridine site.

RBS-Seq signal analysis

We downloaded the raw reads from GSE90963, using reads obtained from RiboMinus-treated total RNA (GSM2418439 and GSM2418440) and polyA-selected RNA (GSM2418443 and GSM2418444). Adapters were trimmed using bbduk. Reads were mapped to hg19 using novoalign, using parameters -t 60 -h 120 -b 4 -H 20 -r A 2 -s 2. For bisulfite-treated samples, the -b 4 parameter was also included. Python scripts using the pysam package were used to determine coverage, the number of deletions, and the number of read 5′ ends at each position, which were then stored as wig files for visualization.

Alternative cleavage and polyadenylation analysis

Analysis of alternative cleavage and polyadenylation was performed with QAPA (Ha et al., 2018), which takes in pseudoalignments. For this purpose we mapped the Illumina RNA-seq reads from WT, PUS1 KO, PUS7 KD and RPUSD4 KD using ENSEMBL GRCh37.75 genome fasta files and Gencode hg19 3′ UTR annotations. Fasta files of 3′ UTR annotations was generated with:

qapa fasta -f genome_fasta_file gencode_3UTR_annotations.bed output_sequences_qapa.fasta

A salmon index was generated with command: salmon index -t output_sequences_qapa.fa -I utr_library. The paired sequencing reads for each sample were then mapped using command: salmon quant.sf -I utr_library -1 ISR -1 Read1.fastq.gz -2 Read2.fastq.gz –validateMappings -o sample_transcript quant. QAPA was then run on samples to quantify polyA site usage (PAU) at annotated 3′UTRs using the following command: qapa quant –db ensembl.identifiers.txt sample_transcript_quant*/quant.sf > PAU_results.txt. We then calculated mean PUA per condition and filtered for >5 TPM in at least 2 samples. An event was classified as an isoform switch if the average difference in PUA between conditions was greater than 10% and the difference between replicates was less than 10%.

Primer extension

Total RNA from WT and PUS1 KO cells was isolated as described above and 20 μg of RNA for each sample was treated with CMC (final concentration 0.1 M) treated and reversed as described. Reverse primers to the U2 snRNA (U2snRNA_ext_sh and U2 snRNA_ext_lo were radiolabeled with γ-ATP (Perkin-Elmer) by treatment with T4 PNK (NEB). Primer extension was carried out with AMV RT (Promega). Briefly, primers were annealed in 1× AMV RT buffer by heating to 90 °C then cooling to 42 °C over 30 minutes in thermocycler. Reverse transcription was carried out at 42 °C for 1 h. Reactions were quenched with 2× stop solution (0.5× TBE, 90% formamide, 0.05% w/v bromophenol blue, 0.05% w/v xylene cyanol). Reactions were then run on 10% TBE–urea PAGE sequencing gel.

QUANTIFICATION AND STATISTICAL ANALYSIS

Statistical analysis was performed in R unless otherwise stated in the methods. Student's T Tests were performed using the t.test() function in R. The hypergeometric tests were performed using the fisher.test(), chisq.test function in R. All other statistics data is specified in the methods and figure legends.